



Recent progress of indoor organic photovoltaics - From device performance to multifunctional applications

Meng-Zhen Sha^a, Yong-Jin Pu^b, Hang Yin^{a,*}, Xiao-Tao Hao^{a,**}

^a School of Physics, Shandong University, Jinan, Shandong, 250100, PR China

^b RIKEN Center for Emergent Matter Science (CEMS), Saitama, 351-0198, Japan



ARTICLE INFO

Keywords:

Indoor organic photovoltaic devices
Photovoltaic molecular design
Fabrication strategies
Multifunctional applications

ABSTRACT

Owing to the prosperity of the internet of things (IoTs), indoor organic photovoltaic (IOPV) devices with substantial merits (e.g., light weight, portability, flexibility, semitransparency, operational stability) are emerging as reliable indoor photon harvesters to drive low-power electronic devices. In such cases, the effective utilization of indoor photons is significant, as indoor light intensity is much weaker than the standard 1-Sun illumination. Considerable efforts have been devoted to improving the power conversion efficiency (PCE) of indoor solar cells and modules in past few years. So far, the efficiency of indoor light harvesters has surpassed 30%, sufficient to power quite a few indoor off-grid electronic devices. Given that the expected efficiency optimization has already realized through various approaches, a critical review is significant for the appropriate applications of IOPV devices. Herein, we provide a detailed review of the basic knowledge of IOPV devices, current fabrication strategies, and further illustrate their multifunctional applications. Possible challenges and prospects of IOPV systems are presented elaborately for further developments and applications.

1. Introduction

Rapid process of modernization causes gigantic energy demands and further leads to global energy crisis [1,2], and the exploration of renewable resource especially clean energy becomes priority throughout the world [3,4]. As naturally inexhaustible clean resource, solar energy is a superior alternative to fossil fuels and solar photovoltaic industry have achieved unprecedented blooming in recent years: according to International Energy Agency's statement, the installed capacity of global photovoltaic reached to 170 GW in 2021, and the global annual increment of solar photovoltaics is expected to reach 422 GW by 2030. Solar energy has exhibited broad developing prospect and is undoubtedly hopeful to alleviate the increasingly serious energy shortage problems. Their large-scale industrialization is inseparable to laboratory experiment efforts and solar cells have gained significant research attentions in recent years with the advancement of various types of photovoltaic systems (see Fig. 1).

Among various photovoltaics devices such as crystalline/poly-crystalline silicon (c-Si) based solar cells, dye-sensitized solar cells (DSSCs), and perovskite-based solar cells (PSCs), organic solar cells

(OSCs) stand out because of impressive advantages involving adjustable energy level [5–9], lightweight, nontoxicity, low-cost, flexibility and roll-to-roll production [10–19]. So far, OSCs have made great progress in material design [20–41], ternary strategy [42–52], morphology control [53–65], additive-assisting effects [66–68], and interface engineering [69–74]. Impressively, the device performance has reached certified PCE of over 19% for single-junction OSCs by Min's group [75], and surged to 20.2% for tandem organic solar cells by applying intermediate transport layer TiO_x/PEDOT:PSS [76], opening up the 20% era for OSCs. Even though outstanding device performance realized in laboratory, inherent shortcomings (e.g., instability to ambient light and temperature), the cruel external operating environment and the non-available sunlight in cloudy days greatly hindered the practical outdoor applications for OSCs [77]. Compared to the changeable and unstable outdoor environment, relatively mild and steady indoor illuminations exhibit broad developing prospects of the indoor photovoltaic devices. Moreover, the thriving evolution of the IoTs in recent years has made an increasing number of electronic devices (e. g. wireless sensors, watches, calculators, bluetooth) and end nodes (monitors, remote control, actuators) connected to the internet at an unprecedeted speed

* Corresponding author.

** Corresponding author.

E-mail addresses: hyin@sdu.edu.cn (H. Yin), haoxt@sdu.edu.cn (X.-T. Hao).

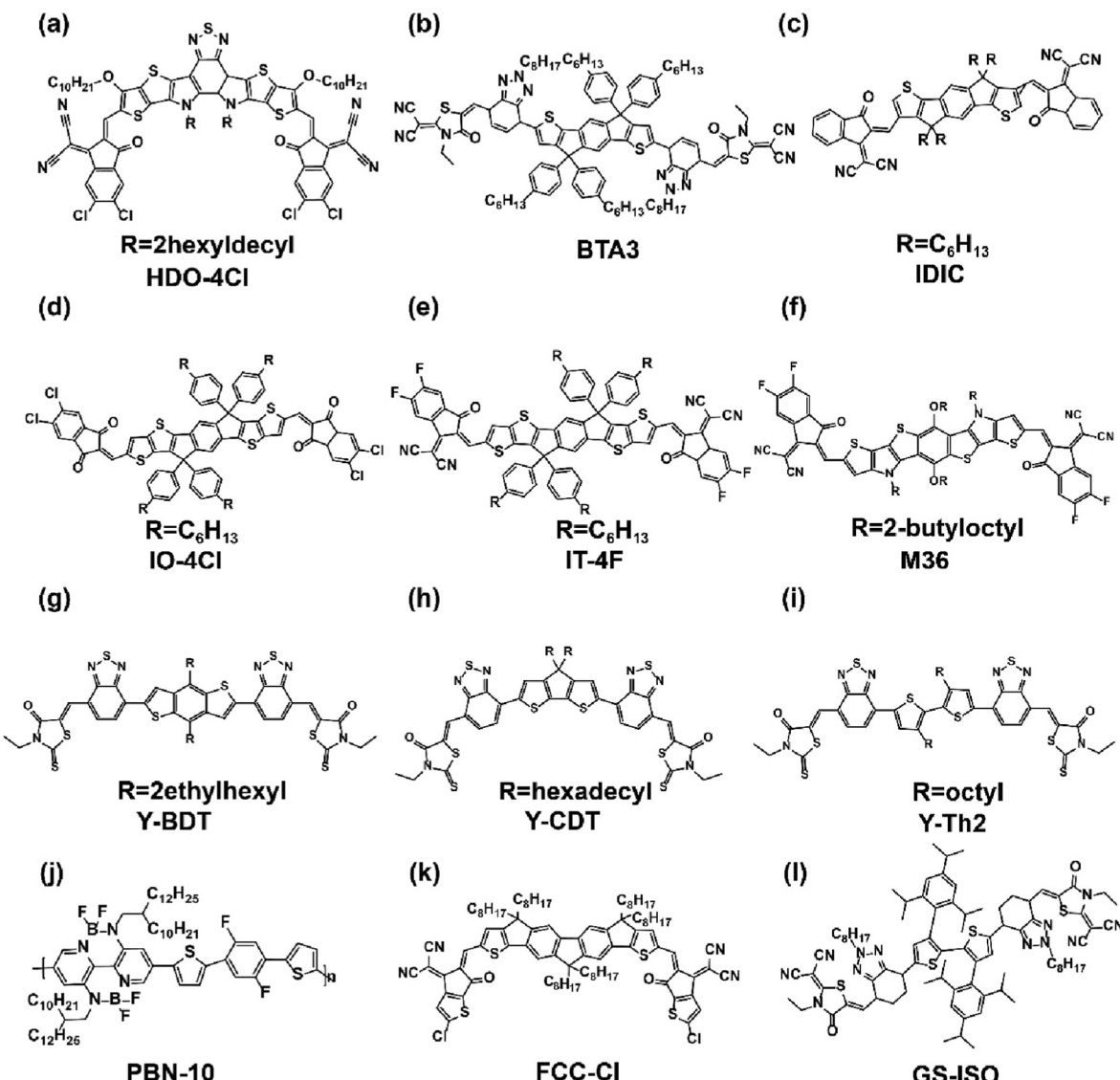


Fig. 1. Selected chemical structures of acceptor materials for indoor OPV devices.

which immensely facilitates the progress of indoor photovoltaic (IPV) cells [78].

Capable of converting the indirect stray sunlight or indoor artificial light into electricity directly, IPV cells can serve as sustainable power sources to drive electronics and they are springing up rapidly in the past few years [79–81]. The IPV device is an amicable and sustainable technology for the supplying of continuous and environmentally-friendly energy source without excessive cautious care and device management. Ho et al. has demonstrated the SQ-limited efficiencies η_{SQ} for various indoor light sources under 300 lux can reach a maximum value of ~57% with the bandgap energies E_g between 1.82 and 1.96 eV (681–632 nm) [82], significantly higher than the AM 1.5G conditions (~33% at 1.1 eV) and this result is almost independent on the type of light sources and illuminance levels. Meanwhile, the SQ-limited output power intensity could reach $41 \mu\text{W cm}^{-2}$ at 300 lux and $136 \mu\text{W cm}^{-2}$ at 1000 lux, respectively, which are sufficient to power different IoTs [88]. In the past few years, c-Si based IPV cells [83], DSSCs-based IPV cells [84] and PSCs-based IPV cells [85] have been gradually employed into indoor photon harvesting except for sunlight collecting and obtained fantastic achievements. The amorphous silicon based IPV cells can exhibiting the maximum output power of $25.56 \mu\text{W cm}^{-2}$ under a 500 lux FL irradiation with long-lived stability irradiation [86].

Co-sensitized DSSC-based IPV cells have produced the highest record PCE of 31.80% under a 1000 lux FL lamp [87]. PSCs-based IPV cells demonstrated a recorded PCE of 35% benefiting from passivated surface traps and elevated electron extraction [88]. Nevertheless, IOPV devices stand out among various indoor photovoltaics because of three striking advantages. First, organic photovoltaic (OPV) exhibits huge potential as reliable and suitable indoor energy harvesters because of the tailorable structure properties of organic materials realized through molecular engineering such as modification on end/terminal groups, side chain and core skeletons. And this kind of property could provide a vast number of organic materials for indoor application [89–93]. Moreover, benefiting from the tuneability of band gaps via chemical design, the absorbance of the active layer materials could be tuned to match various light sources. Furthermore, although the much weaker light intensity indoor (~200–1000 lux) compared to the standard AM 1.5G illumination (~100,000 lux) [94–97], the photo-stability property of IPV devices is better and meanwhile an elevated PCE can be obtained under indoor conditions [98], demonstrating huge developing space [99–101]. IOPV devices has gained well-pronounced developments in recent years. In 2015, Cutting et al. illustrated that OPV devices can outperform c-Si based counterparts under indoor artificial light conditions, showing a great potential for indoor energy harvesting [102]. In 2017, Lee et al.

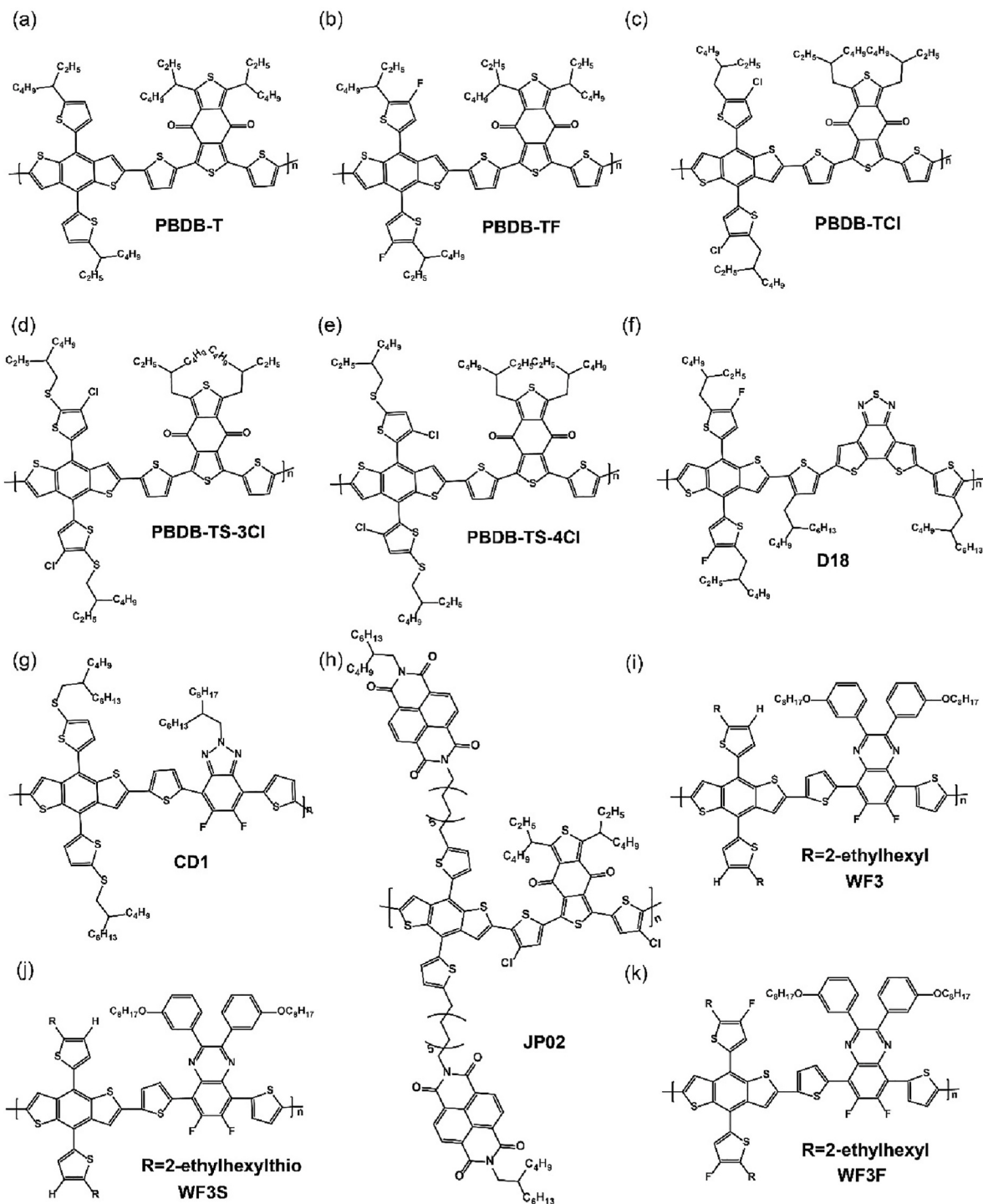


Fig. 2. Selected chemical structures of donor materials for indoor OPV devices.

found that the BTR:PC₇₁BM based solar cells can deliver admirable device performance with a champion efficiency over 28% under FL lamp benefiting from balanced crystallization and phase separation properties [103]. Subsequently, the wide-bandgap polymer donor PBDB-T and its derivatives are gradually adopted as the commonly used material for indoor light harvesting combined with different acceptors [104] and realized satisfactory device performance [105]. Furthermore, narrow bandgap non-fullerene acceptor with excellent photovoltaic performance under the standard AM 1.5G condition are frequently applied for indoor applications with excellent achievements in recent years [106, 107]. The PCE of the IOPV cells can be further optimized for practical

applications, and till now the PCE has reached 30.8% under 1650 lux LED lamp [108], which suggests OPVs are promising indoor power sources.

Besides the remarkable achievements realized in device performance, intrinsic properties of organic semiconductors such as the flexibility and semitransparency endow IPV devices with special application potentials. IOPV cells have displayed broad prospects in practical applications such as building integrated photovoltaic modules [109], chromaticity manipulation and wearable devices [110]. For their future advance in the fields of portable and wearable carry-on electronics, large-area and flexible devices, self-powered semi-transparent

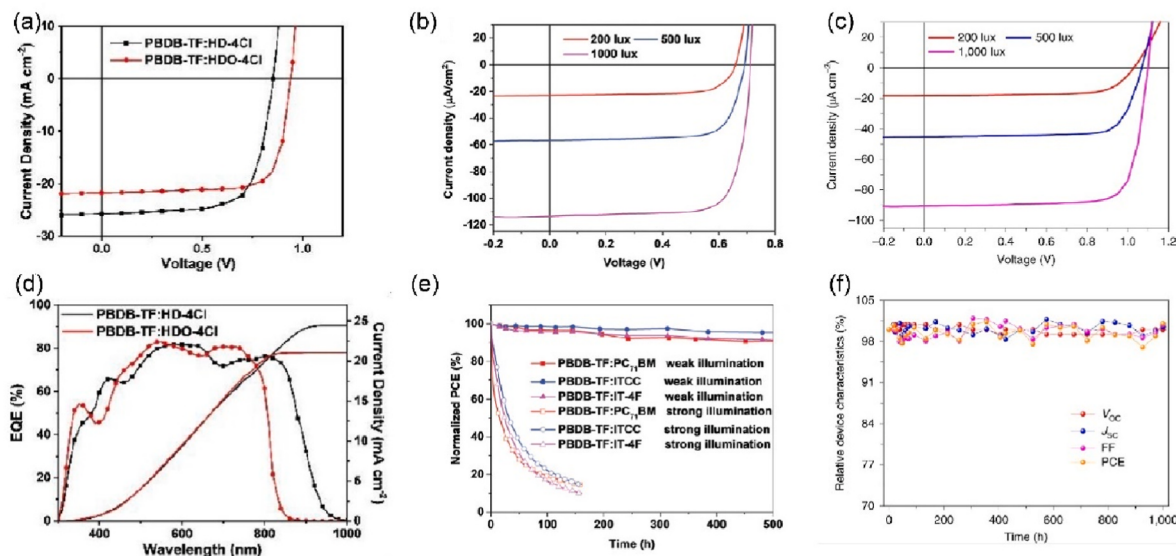


Fig. 3. (a) J-V characterizations of the PBDB-TF:HDO-4Cl based OPV cells under warm white LED (2700 K) illumination with varied light intensities of 200, 500, and 1000 lux. Reprinted with permission from ref. 114 (copyright The Royal Society of Chemistry 2021). (b) PBDB-TF:IT-4F based OPV cells under warm white LED (2700 K) illumination with varied light intensities of 200, 500, and 1000 lux. Reprinted with permission from ref. 115 (copyright John Wiley & Sons 2019) (c) PBDB-TF:IO-4Cl based OPV cells under warm white LED (2700 K) illumination with varied light intensities of 200, 500, and 1000 lux. Reprinted with permission from ref. 116 (copyright John Wiley & Sons 2021). (d) EQE responses of PBDB-TF:HDO-4Cl. (e) The stability of PBDB-TF:IT-4F photovoltaics. (f) The curves of the photovoltaic characteristics versus time about the PBDB-TF:IO-4Cl based OPV cells.

photovoltaics with aesthetic comfort, it is of utmost importance to clarify the underlying physical mechanism and summarize corresponding applications achievements.

In this contribution, we summarized recent achievements of indoor organic photovoltaics from device performance to multifunctional applications. We first expound on the general knowledge of IOPV devices from the photoactive layer material selection to the fundamentals of accurate measurements. Thereafter, different PCE optimization

strategies in recent years are summarized elaborately from the aspects of the ternary strategy, trap state controlling strategy, and interfacial engineering strategy. Moreover, as the strikingly flexible and semi-transparent properties of OPV devices, we further discussed their multifunctional applications in daily life including the fabrication requirements and recent progress of indoor flexible device, the general knowledge and latest achievements about semi-transparent IOPV devices. Finally, the potential challenges and opportunities are put forward

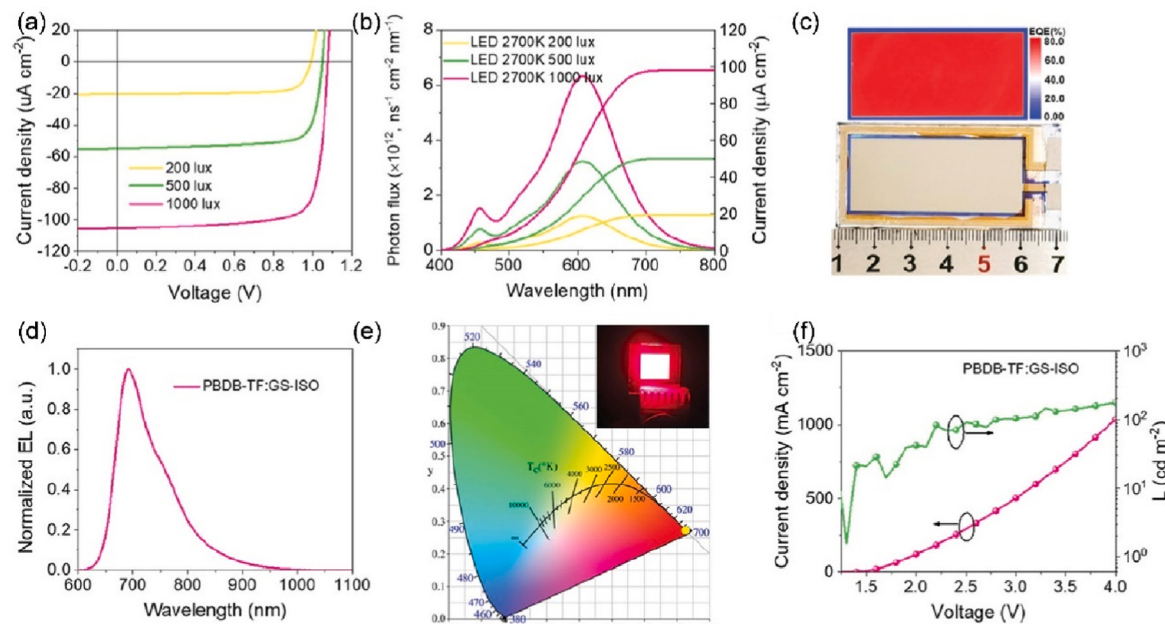


Fig. 4. (a) J-V curves of the device based on PBDB-TF:GS-ISO under 200, 500, and 1000 lux, 2700 K LED. (b) Photon fluxes and the corresponding integral current densities of the 2700 K LED bulb. (c) The digital photo and EQE mapping image of the 1 cm² PBDB-TF:GS-ISO-based cell. (d) The EL spectra of PBDB-TF:GS-ISO-based cell. (e) The color coordinates of PBDB-TF:GS-ISO-based cell. (f) J-V-L curves of the device based on PBDB-TF:GS-ISO. Reprinted with permission from ref. 117 (copyright John Wiley & Sons 2022).

Table 1

Detailed photovoltaic parameters of the OPV cells.

Photoactive layer	light source	Luminance [lx]	HTL	ETL	V_{OC} [V]	J_{SC} [$\mu A\text{ cm}^{-2}$]	FF [%]	PCE [%]	P_{out} [$\mu W\text{ cm}^{-2}$]	ref
PBDB-TF:HDO-4Cl	LED	1000	PEDOT: PSS	PFN-Br	0.793	120.2	75.7	23.4	72.2	[114]
PBDB-TF:IT-4F	LED	1000	PEDOT: PSS	PFN-Br	0.712	113.0	78.0	20.8	62.8	[115]
PBDB-TF:IO-4Cl	LED	1000	PEDOT: PSS	PFN-Br	1.100	90.6	79.1	26.1	78.8	[116]
PBDB-TSCL:IT-4F	FL	500	MoO ₃	ZnO	0.630	60.4	76.3	21.5	29.1	[121]
PBDB-TS-4Cl:IT4F	FL	500	MoO ₃	ZnO	0.640	64.9	73.9	21.7	31.0	[122]
PBDB-TS-3Cl:IT4F	FL	500	MoO ₃	ZnO	0.640	62.8	72.2	20.4	29.2	[122]
WF3F:PC ₇₁ BM	LED	500	MoO _x	ZnO	0.690	63.6	67.4	17.3	–	[123]
JP02	LED	1000	MoO ₃	ZnO/PFN-Br	0.790	95.1	73.0	19.4	56.7	[125]
C8TEBDT-2P:IDIC	LED	300	PEDOT: PSS	ZrAcac	0.590	24.6	62.5	12.3	–	[126]
PBDB-TF:GS-ISO	LED	1000	PEDOT: PSS	PFN-Br	1.090	101.5	80.4	29.1	88.9	[117]
D18:FCC-Cl	LED	500	MoO ₃	ZnO	0.936	61.6	79.5	28.8	45.8	[118]
S2:LBT-SCI	LED	1000	PEDOT: PSS	PNDI-F3N	0.864	125.0	74.1	25.1	80.0	[119]
CD1:PBN-10	FL	1000	PEDOT: PSS	Ca	1.140	120.0	66.2	26.2	91.0	[120]
PM6:Y6:Y-Th2	LED	1000	PEDOT: PSS	PDINO	0.703	32.3	75.1	22.7	16.6	[137]
PCDTBT:PTB7:PC ₆₁ BM:	LED	500	MoO _x	PFN	0.603	46.0	76.6	10.6	18.3	[138]
PC ₇₁ BM										
PCDTBT:PDTSTPD:PC ₇₁ BM	FL	300	PEDOT: PSS	LiF	0.730	33.3	63.5	20.8	15.4	[104]
PTB7:PC ₇₁ BM:EP-PDI	LED	500	MoO _x	ZnO	0.650	57.0	68.5	15.7	–	[134]
J52-F:PM7:BTA3	LED	500	PEDOT: PSS	Ca	1.000	26.5	68.1	20.0	–	[133]
PM6:M36	LED	2000	PEDOT: PSS	PDINO	0.800	268.0	67.4	19.5	–	[148]
PBDB-T:BTA3	LED	1000	PEDOT: PSS	PFN-Br	0.990	98.5	73.6	23.3	71.8	[149]

for their further breakthroughs in the near feature.

2. Basic knowledge and progress of IOPV device

2.1. Material design strategy

Unlike the standard 1-Sun illumination which contains a broad irradiation spectrum from 400 nm to 2000 nm including ultraviolet, visible and infrared light, the emission spectrum of indoor artificial light lies in the visible region (400–750 nm) with lower light intensity (<1 mw cm^{-2}) compared to the AM 1.5G cases (100 mw cm^{-2}). Therefore, the material selection strategy is different in both cases. Active layer materials for indoor applications should be carefully selected to make the best use of indoor photons, and this often requires the absorbance of the materials covering the wavelength range from 400 nm to 750 nm

with strong absorbance, which matches well with the indoor irradiation spectra (mainly released by LED bulb and FL tube). Polymer donor PBDB-T and its derivatives are frequently applied in IOPVs because of suitable bandgap for indoor photon harvesting, high absorption capacity as well as great carrier mobility [111]. Besides, as the indoor light intensity is much weaker compared to the AM 1.5G condition, leakage current and trap-assisted recombination become more dominant and greatly affect the overall device performance of indoor devices. As a result, materials possessing less traps are more suitable for the suppression of leakage current [112,113]. Furthermore, on account of the smaller open-circuit voltage (V_{OC}) under indoor condition, the PCE always suffers a great loss compared to the 1-Sun case. Thus, solar cells with high V_{OC} values under indoor conditions should be exactly needed. All the above considerations put forward the molecular design and seek for perfect indoor organic active materials (see Fig. 2).

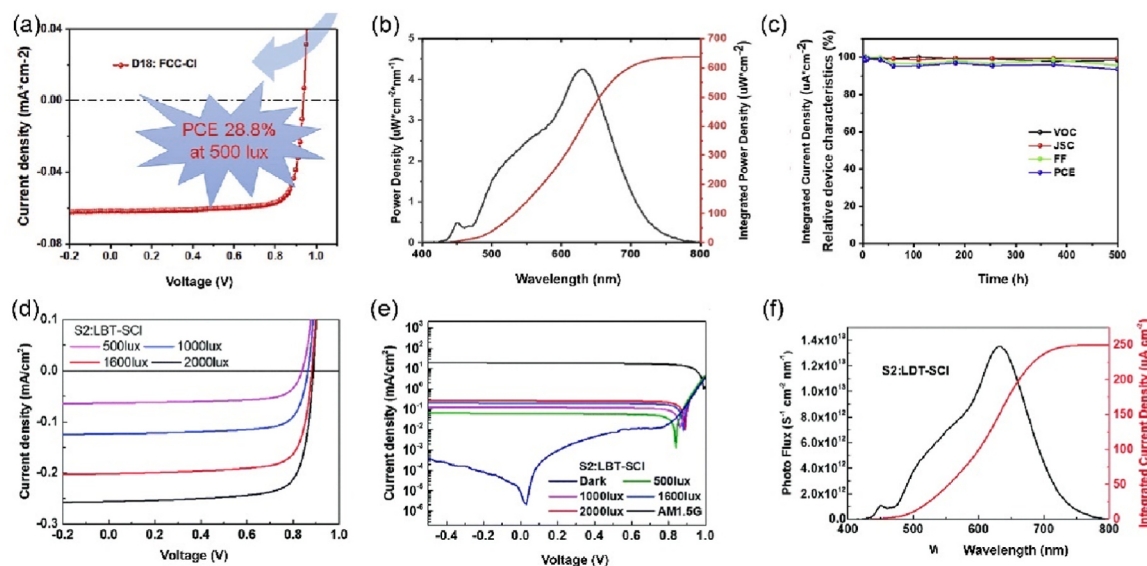


Fig. 5. (a) The J-V curves of D18:FCC-Cl under 500 lux LED irradiations, (b) The emission power spectrum and integrated power density curve of the 2600 K LED at 2000 lux. (c) The normalized device parameters for D18:FCC-Cl versus time under different LED light sources. Reprinted with permission from ref. 118 (copyright Elsevier 2021). (d) J-V curves of the OPVs based on S2:LBT-SCI under different indoor light intensity. (e) The current density as a function of voltage based on S2:LBT-SCI under different light conditions. (f) The photo flux spectrum of the 2600 K LED lamp at 2000 lux and the integral current density of the OPVs based on S2:LBT-SCI under that condition. Reprinted with permission from ref. 119 (copyright Royal Society of Chemistry 2021).

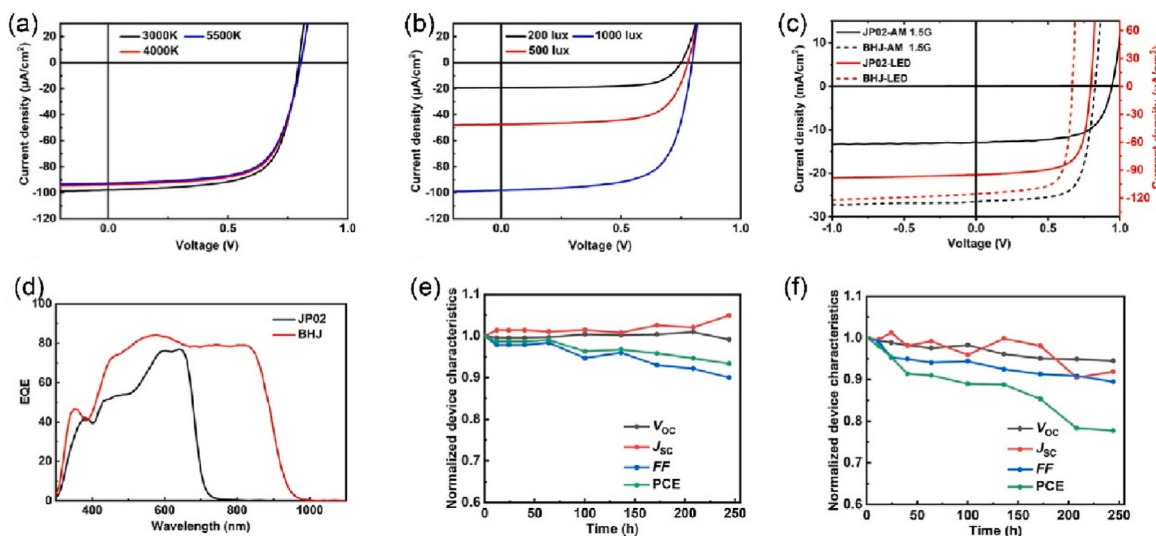


Fig. 6. (a) Characterizations of JP02-based SCOSCs, (A) J-V curves under different LED light sources. (b) J-V curves under different illumination intensities in LED 3000 K light source. (c) J-V curves of JP02 based (solid line), BHJ photovoltaic cells (dashed line) under LED light source and AM1.5G light source. (d) EQE of the OSC devices. (e) Normalized V_{oc} , J_{sc} , FF, and PCE (average values) decay of JP02-based SCOSCs and (f) PM6:BTP-BO-4Cl-based BHJ-type OSCs. Reprinted with permission from ref. 125 (copyright John Wiley & Sons 2021).

In 2021, Hou and co-workers synthesized a wide-bandgap non-fullerene acceptor HDO-4Cl by modifying HD-4Cl [114]. HDO-4Cl has smaller electron affinity which assisting to gain an undamaged V_{oc} value under indoor condition, and a desirable PCE of 23.4% was acquired under 1000 lux LED irradiation by using PBDB-TF and HDO-4Cl as active layer materials (Fig. 3a). Moreover, they used a wide-bandgap polymer donor PBDB-TF and a low-bandgap acceptor IT-4F to fabricate the OPV cell and achieved an impressive PCE value of 20.8% under 1000 lux LED illumination just as shown in Fig. 3b [115]. Particularly, it worth noting that the device retained 95% of its original PCE value when exposing to continuous illumination up to 500 h (Fig. 3e), which implies great device stability of indoor devices. Simultaneously, they rationally synthesized an acceptor IO-4Cl and blended it with PBDB-TF, and the binary system enjoyed strong absorbance from 400 nm to 700 nm and shows high (EQE_{EL}) values. Under a 2700 K LED light condition, the PCE of the device reached 26.1% and realized good stability in practical applications (Fig. 3c and f) [116]. Concomitant accurate measurement in the process ensured the reliability of the PCE results in above three works. Besides, Hou et al. also applied the wide-bandgap NFAs GS-ISO for indoor applications and exhibit a PCE of 29.15% under 1000 lux LED illuminations with a large device area of 1 cm^2 [117]. Moreover, the 1 cm^2 cell shows an electroluminescence (EL) peak located at 690 nm (Fig. 4d) and a chromaticity coordinate of (0.73, 0.27) (Fig. 4e). The J-V-L curves in Fig. 4f manifests a luminance of 178 cd m^{-2} at 4 V and a turn-on voltage below 1.5 V which verified its great potential working as LED. It is worth mentioning that they further fabricated PBDBTF: GS-ISO-based cell with an area of 10.0 cm^2 (Fig. 4c) which is hopeful for applying in large-area OPV cells. Corresponding parameter information is shown in Table 1.

Yan et al. recently synthesized a high crystalline small molecular acceptor FCC-Cl and achieved an impressive PCE of **28.8%** under 500 lux LED illuminations when blending with D18 as depicted in Fig. 5a-c [118]. Further, by modifying Y6, they reported two novel NFAs called LBT-DF and LBT-SCl, and particularly, LBT-SCl gained an overall efficiency of 25.1% under indoor conditions (Fig. 5d) [119]. As for polymer acceptors, Liu and co-workers reported all-polymer indoor organic solar cells base on CD1:PBN-10 and achieved the PCE of 26.2% under fluorescent lamp illumination with relatively high V_{oc} value up to 1.14 V [120].

On the foundation of the PBDB-TF, Son and co-workers synthesized its derivative PBDB-TSCL which possesses more efficient exciton disso-

ciation and charge generation, exerting great influence on subsequent photovoltaic performance. Consequently, PBDB-TSCL based device attained the PCE as high as 21.53% with the FF of 76.29% under a 500 lux fluorescence lamp, and showed improved thermal stability [121]. Apart from the PBDB-TF, they recently synthesized a series derivatives of PBDB-TS named PBDB-TS-3Cl and PBDB-TS-4Cl through chlorination, devices based on the above two polymers show optimized morphology, decreased leakage current and improved V_{oc} values which bring forth the enhancement of PCE in both the standard 1-Sun irradiation and indoor light sources [122]. Ultimately, when blending the PBDB-TS-4Cl with IT-4F the PCE of the device reached 21.7% with the FF of 73.9% under 500 lux fluorescence irradiation. Table 1 summarizes results of the above typical works.

Besides the PBDB-TF based donor materials, Lee and co-workers synthesized three conjugated polymer donors WF3 WF3S WF3F and blended them with PC₇₁BM to fabricated IPV devices [123]. Combined advantages of suppressed trap-induced energy loss, balanced charge transport and desirable nanoscale morphology, the WF3F: PC₇₁BM achieved an efficiency of 17.34% under a 500 lx LED source. Furthermore, the fluorinated phenylene-alkoxybenzothiadiazole-based wide bandgap polymer donor PDTBTBz-2Fant was introduced to indoor conditions by Shim and co-workers and realized the PCE value of 23.1% when blending with PC₇₁BM under LED illuminations [124].

As single-component materials exhibit excellent thermostability and photostability, they are also good candidates for indoor applications. Lately, the emergence of single-component materials with the structure of double-cable satisfied the requirements for indoor devices. These materials often show rather low leakage current and less trap-induced recombination compared to BHJ materials [125]. Li and co-workers used the wide-bandgap double-cable single-component material JP02 to fabricate the inverted indoor organic solar cells and it demonstrated a high PCE of 19.44% under 1000 lux LED lamp. Albeit the performance of JP02 fell behind the PM6:BTP-BO-4Cl based BHJ under same indoor conditions, JP02 based device presented better stability, and its PCE retained 93.9% of the original value after 244 h (Fig. 6).

Porphyrins and their derivatives are naturally strong light harvesters and thus can be effectively utilized in organic photovoltaics. Furthermore, their properties of slightly weak absorption in the range from 550 nm to 700 nm endow them the potential for high-transparency indoor photovoltaics. Zhu and co-workers used two porphyrin dimers C8TEBDT-2P and C8TBDT-2P to fabricate IOPVs with the non-fullerene

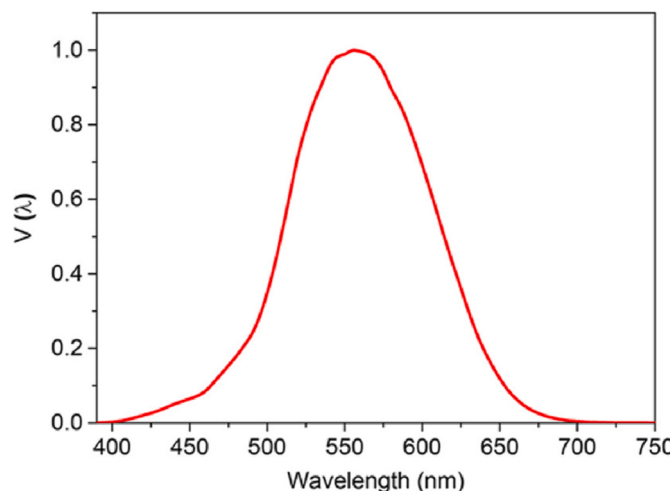


Fig. 7. CIE photopic luminous efficiency functions. Reprinted with permission from ref. 130 (copyright The American Chemical Society 2020).

acceptor IDIC, and the binary system C8TEBDT-2P:IDIC achieved the promising PCE of 12.3% under 300 lux LED lamp because of combined effects such as efficient charge generation and transport, excellent morphology and charge recombination properties [126]. Relevant photopic measurements have shown that the average visible transmittance (AVT) is over 70% for both devices which implies broad application prospect in semi-transparent indoor organic photovoltaics. All the data above further illustrate polymer structure of the active layer materials can have a far-reaching impact on the device performance.

2.2. Basic parameters and accurate measurements

Common descriptions on light intensity are different between AM 1.5G conditions and indoor cases because the light intensity of the latter ($<1 \text{ mw cm}^{-2}$) is less than 1% of the former (100 mw cm^{-2}). With respect to AM 1.5G conditions, the power density of the sunlight (P_{in}) is to depict the light intensity and can be calculated by Equation (1) where

$E(\lambda)$ is the power density spectrum of the sunlight and λ is the wavelength. While for indoor applications, light intensity is expressed by irradiation E_V as shown in Equation (2) [127], where constant K_m is 683 lm/w representing the limitation of human visual light perception, $E_\lambda(\lambda)$ refers to the absolute incident power density spectrum and $V(\lambda)$ stands for the photopic luminous efficiency function of human eye manifesting the average spectral sensitivity of visual perception of the human eye verified by CIE in 1931 (see Fig. 7).

$$P_{in} = \int_0^{\infty} E(\lambda) d\lambda \quad (1)$$

$$E_V = K_m \int_0^{\infty} E_\lambda(\lambda) V(\lambda) d\lambda \quad (2)$$

In analogy to the AM 1.5G conditions, short-circuit current density (J_{sc}), V_{oc} , fill factor (FF) and P_{in} are also four vital factors for indoor applications considering their synergetic effect on the PCE as shown in Equation (3).

$$PCE = \frac{J_{sc} \times V_{oc} \times FF}{P_{in}} \quad (3)$$

Shockley equation is applied to describe the relationship between current density and voltage:

$$J = \frac{R_{sh}}{R_{sh} + R_s} \left\{ J_0 \left[\exp \left(\frac{q(V - JR_s)}{nkT/q} \right) - 1 \right] + \frac{V}{R_s} \right\} - J_{ph} \quad (4)$$

where R_{sh} , R_s , J_0 , J_{ph} , k , and n are series resistance, shunt resistance, reverse saturation current density, generated photocurrent density, Boltzmann's constant, and diode ideality factor respectively. Caused by the dim indoor irradiation, the J_{sc} in indoor environments is much lower than the AM 1.5G case and the low J_{sc} could eliminate the negative effect of large R_s on device performance. Furthermore, the weak irradiation indoor endows the device of long-term stability and the potential for thick-film fabrication [121,128,129].

According to Shockley equation [130], V_{oc} is evolved to Equation (5) by supposing $R_{sh} \gg R_s$ which can be expressed as:

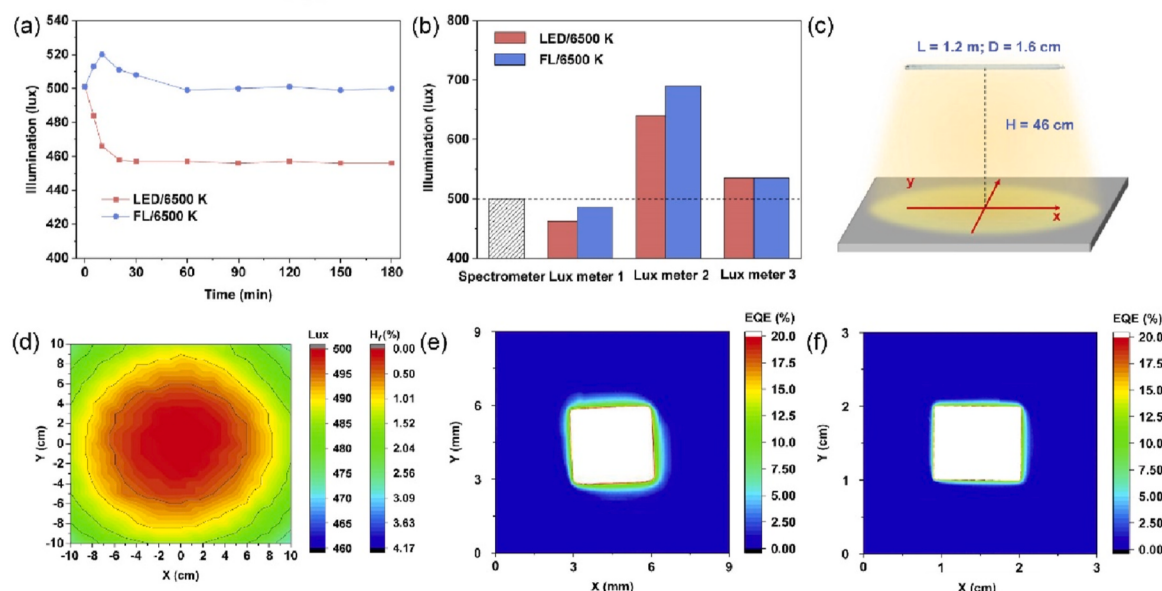


Fig. 8. Comparison, light power distribution and the EQE distribution of light sources. (a) The illuminations of the 6500 K LED bulb and 6500 K FL tube continuously working for 3 h. (b) Comparison of illuminations of the three lux meters and the spectrometer under the 6500 K LED bulb and 6500 K FL. (c) A 6500 K LED bulb used in experiment. (d) Light power distribution of the 6500 K LED bulb. (e) EQE mapping image of the 9.80 mm² device w/o a mask. (f) EQE mapping image of the 1.07 cm² device w/o a mask. Reprinted with permission from ref. 127 (copyright Elsevier 2021).

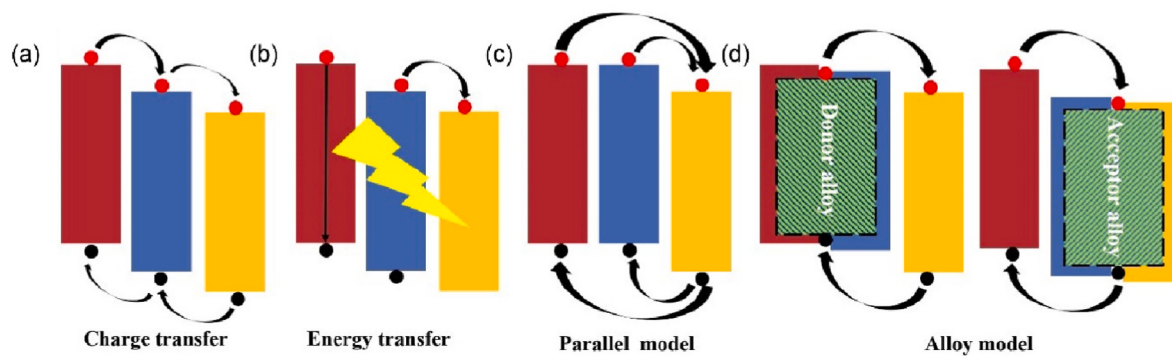


Fig. 9. Working mechanism of the ternary organic solar cells. Reprinted with permission from ref. 131 (copyright John Wiley & Sons 2019).

$$V_{oc} \approx \frac{nkT}{q} \ln \left(\frac{J_{ph}}{J_0} + 1 \right) \quad (5)$$

The value of n can reflect the recombination mechanism in photovoltaic device. The recombination can be neglected when $n = 1$ while obvious when $n = 2$. A dim indoor illumination would give rise to the broadening of the electronic density of states (DOS) and emerge of defect level which aggravating recombination effects. Compared with the AM 1.5G illumination, n becomes larger here and the combined low J_{ph} value creates smaller V_{oc} value under indoor illuminations.

Kippelen et al. put forward the following three equations to explain the correlation between light intensity and FF. Just as shown in Equations (6)–(8), FF has different expressions under various conditions. Equation (6) displays an ideal FF namely FF_0 . FF evolves to FF_s (Equation (7)) under the condition $v_{oc} > 10, r_s < 0.4, \frac{1}{R_{sh}} = 0$, where in this case FF is mainly dependent on R_s . However, under low illumination conditions (J_{sc} is lower than $10^{-2} \text{ mA cm}^{-2}$, $R_{ch} \gg R_s$ and r_s is negligible) FF is mainly corrected with R_{ch} and thus FF would turn into FF_{sh} (Equation (8)).

$$FF_0 = \frac{v_{oc} - \ln(v_{oc} + 0.72)}{v_{oc} + 1} \quad (v_{oc} > 10, R_s = \frac{1}{R_{sh}} = 0) \quad (6)$$

$$FF_s = FF_0 (1 - r_s) \left(v_{oc} > 10, r_s < 0.4, \frac{1}{R_{sh}} = 0 \right) \quad (7)$$

$$FF = FF_{sh} = FF_s \left[1 - \frac{(v_{oc} + 0.7)FF_s}{v_{oc}r_{sh}} \right] \left(v_{oc} > 10, r_s + \frac{1}{R_{sh}} < 0.4 \right) \quad (8)$$

where $v_{oc} = \frac{qV_{oc}}{nkT}, r_s = \frac{R_s}{R_{ch}}, r_{sh} = \frac{R_{sh}}{R_{ch}}, R_{ch} = \frac{V_{oc}}{A J_{sc}}$. v_{oc} is the normalized V_{OC} , r_s is the normalized R_s , r_{sh} is the normalized R_{sh} , and R_{ch} is the characteristic resistance for the device which represents the output resistance of the OPV operating at maximum power. A is the effective area of the device [127]. As Equation (8) depicts, FF would monotonically increase with the intensity of light under rather low illuminations. Nevertheless, Kippelen et al. revealed that further increment of light intensity would cause the drop of FF due to the non-negligible r_s in high illuminations. Relatively high FFs for IOPV devices relative to the AM 1.5G condition have already been confirmed in experiments.

P_{in} is also a vital part determining the overall device performance. However, unlike solar simulator which supply fixed light intensity calibrated by standard silicon solar cells, multiply light sources (LED, FL, halogen lamp) and non-uniform testing standard for indoor application cause inaccurate measurements of P_{in} and further influence the testing reliability of PCE values. Hou and co-workers pointed out the reasons for

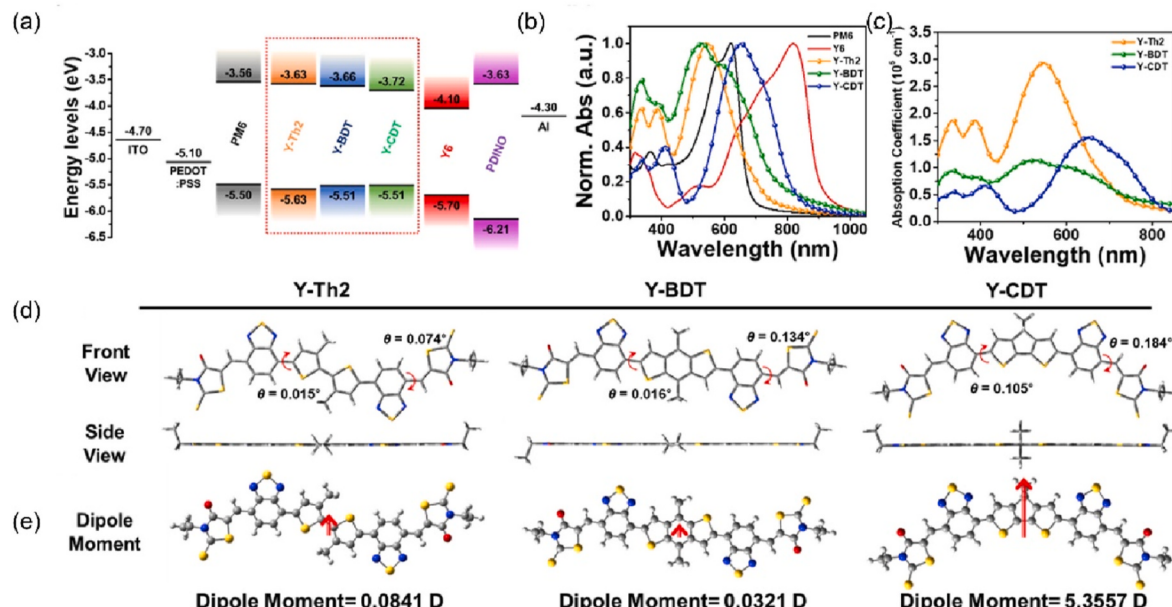


Fig. 10. (a) Energy level diagram of materials utilized for the photovoltaic devices. (b) Normalized UV-Vis absorption spectra of active layer components and (c) Y-acceptors in thin films. (d) Optimized geometries of Y-Th2, Y-BDT, and Y-CDT by DFT calculation. (e) Dipole moments of the three materials. Reprinted with permission from ref. 137 (copyright Elsevier 2020).

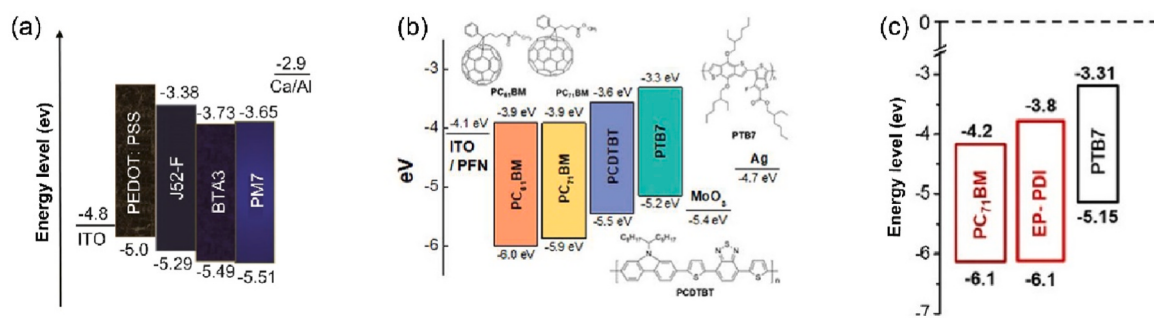


Fig. 11. (a) Energy level diagram for J52-F:PM7:BTAA3 based ternary indoor organic photovoltaics. Reprinted with permission from ref. 133 (copyright Elsevier 2021). (b) Energy level diagram for PCDTBT:PTB7:PC₆₁BM:PC₇₁BM based quaternary indoor organic photovoltaics. Reprinted with permission from ref. 138 (copyright Elsevier 2019). (c) Energy level diagram for PTB7:PC₇₁BM:EP-PDI based ternary indoor organic photovoltaics. Reprinted with permission from ref. 134 (copyright John Wiley & Sons 2019).

inaccurate measurement of P_{in} as shown in Fig. 8. First is the instability of light source intensity. As indoor sources (e.g. LED, FL) are required to connect to the voltage regulator for the acquirement of stable light intensity, but this takes at least 30–60 min until used for normal testing, which would cause inaccurate measurement. Secondly, Fig. 8b reveals that different illuminometer output disparate illumination values compared with the standard spectrograph even at the same measurement place, and therefore, utilizing the illumination value measured by illuminometer to indirectly calculate P_{in} will cause large testing errors. Third, intensity distribution of indoor light source is not uniform except the place at the center of the light source, and thus the spatial place of the light source needs to be carefully adjusted. Finally, edge effect of photovoltaic devices and the influence of stray light further carry out

incorrect P_{in} values.

Based on the above analysis, to get an accurate P_{in} , light source and testing position need to be carefully selected for the acquirement and veracity of homogeneous light power density. Then, P_{in} should be calculated by the integration of optical power density which is measured directly by the spectrometer. Furthermore, a suitable mask aperture and a relatively large effective area of photovoltaics are required to eliminate the edge effect. Finally, the measurement of indoor photovoltaic devices is supposed to carry out in dark environment to remove the influence of stray light.

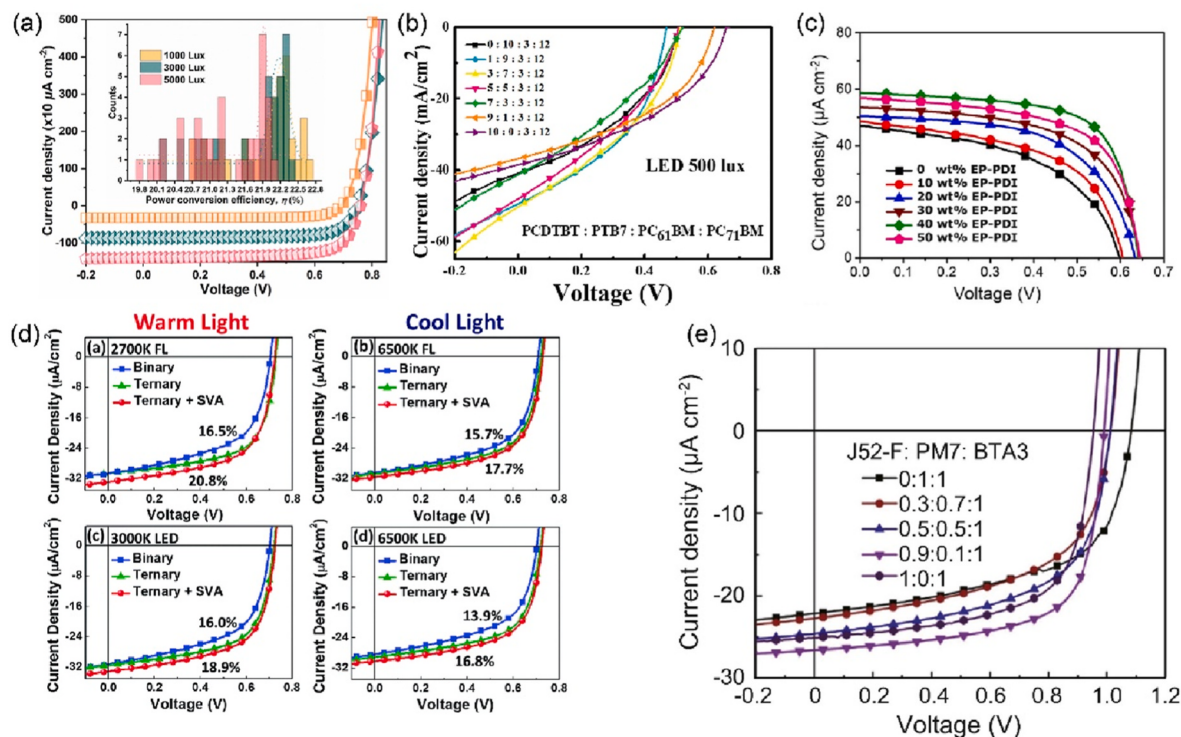


Fig. 12. (a) J-V curves of PM6:Y6:Y-Th2 based OPVs under indoor illuminations of 1000, 3000, and 5000 lux. Reprinted with permission from ref. 137 (copyright Elsevier 2020). (b) J-V curves PCDTBT:PTB7:PC₆₁BM:PC₇₁BM based quaternary OPVs of different composition weight ratios under 500 lx white LED illumination. Reprinted with permission from ref. 138 (copyright Elsevier 2019). (c) J-V curves of PTB7:PC₇₁BM:EP-PDI based ternary photovoltaics with different EP-PDI doping concentrations. Reprinted with permission from ref. 134 (copyright John Wiley & Sons 2019). (d) J-V characteristics of binary PCDTBT:PC₇₁BM and ternary PCDTBT:PDTSTPD:PC₇₁BM OPV devices under different indoor illuminations. Reprinted with permission from ref. 104 (copyright The Royal Society of Chemistry 2018). (e) J-V curves of J52-F:PM7:BTAA3 based OPVs with various proportions under 300 lux LED irradiations. Reprinted with permission from ref. 133 (copyright Elsevier 2021).

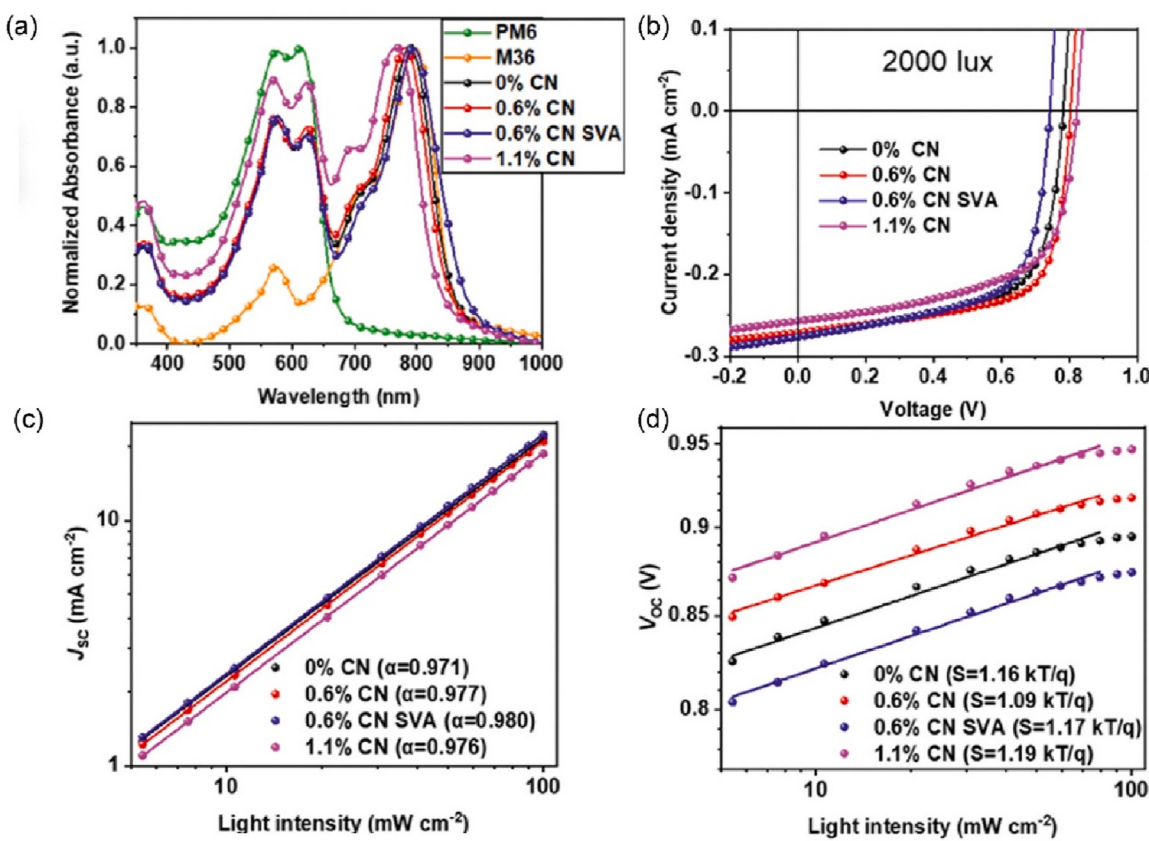


Fig. 13. (a) UV-vis absorption spectra of PM6:M36 OPVs with different conditions. (b) J-V curves of PM6:M36 OPVs. (c) The dependence of current density on light intensity under various conditions for devices. (d) The dependence of open-circuit voltage on light intensity under various conditions for devices. Reprinted with permission from ref. 148 (copyright The American Chemical Society 2021).

2.3. Ternary strategy

Ternary organic solar cells (TOSCs) fabricated by adding an additional third component to the original binary bulk heterojunction (BHJ) system to form two-donor/one-acceptor or one-donor/two-acceptor structure in a single active layer is an effective way to combine the merits of each photovoltaic materials and boost the overall device performance [131]. As depicted in Fig. 9, charge transfer, energy transfer, parallel mode and alloy mode are four fundamental working mechanism of TOSCs. Usually there are one or more advantages in a single TOSCs and they are supposed to improve the performance of the system synergistically.

Once an appropriate third component is added into the binary BHJ film, the device performance could be elevated given that (i) the blending components can complement in absorbance which can make the best use of incident photons; (ii) the energy level cascade effects facilitate the charge generation and thus improve photocurrent and efficiency; (iii) the crystalline and phase separation of the blending films are optimized resulting in desirable charge transport. Besides the meaningful advantages above, TOSCs offer a simple but efficient way to fabricate high-performance thick OSCs compensating the impaired device performance which come with the increasing thickness of the active layers and facilitate the roll-to roll production application of OSCs. Furthermore, long-time stability involving thermal, photo-thermal and air cases could be attained by introducing a proper third component like cross-linkers, fullerene derivatives and non-photosensitive materials [132], manifesting huge potential in commercial production. The ternary strategy is an effective way to improve device performance and has been widely adopted in both the AM 1.5G condition and indoor scenarios [133,134].

The emergence of near-infrared (NIR)-absorbing non-fullerene

acceptor Y6 in 2019 is epoch-making in the OPV field, since then the efficiency of single OPVs has broken 15% [135,136]. In recent years, Y6 has been frequently applied in various OPV cells due to the high absorbance in NIR and narrow bandgap. Till now the PCE of single junction OSC has reached 19% because of the effective utilization of Y-serious (Y1~Y6) NFAs as well as their derivatives. Recently, Yang's group synthesized a series of special Y-series acceptors (Y-Th2, Y-BDT, and Y-CDT) with a dual acceptor-donor-dual acceptor (A1-A-D-A1) structure based on the ring-fused strategy [137]. These three acceptors act as guest acceptors when blending with PM6:Y6. Resulting from the complementary absorbance and the cascade energy level, the device performance improved when Y-TH2 or Y-BDT were introduced to the system with an optimal amount in contrast to the initial binary blends. The PCE of the Y-Th2 based cell reached 22.7% under a 1000 lux LED due to the cascade energy level alignment (Fig. 10a), high absorption coefficient in short-wavelength region (Fig. 10b and c), quite planar configuration (Fig. 10d and e), effective charge generation and improved charge-carrier mobilities. The results show the performance of all the ternary organic solar cells enhanced with different Y-Th2 contents.

The traditional fullerene acceptor PC₇₁BM is frequently applied for indoor applications in recent years. So and co-workers have employed several polymers into the binary system PCDTBT:PC₇₁BM for further performance improvement and achieved the PCE of 20.8% based on the ternary system of PCDTBT:PDTSTPD:PC₇₁BM because of enhanced hole mobilities and reduced Urbach energies [100]. Based on the binary system PTB7:PC₇₁BM, Lee et al. added the monomeric perylene diimide (PDI) small molecules called EP-PDI to fabricate ternary photovoltaics. Fig. 11c depicts the favorable energetics in the ternary case which implies PTB7 could act as an electron donor to both PC₇₁BM and EP-PDI, promoting charge transfer to some extent. Benefited from the

Table 2

Structure Parameters of the Corresponding Films Obtained from GIWAXS and RSoXs. Reprinted with permission from ref. 148 (copyright The American Chemical Society 2021).

condition	d-spacing (Å)	CL (Å)	domain size (nm)	domain purity
0% CN	3.76	23.89	22.3	0.95
0.6% CN	3.79	24.88	21.6	0.99
0.6% CN SVA	3.81	39.49	24.4	1

favorable energetics and elevated morphology, the ternary blends PTB7:PC₇₁BM:EP-PDI eventually achieved a PCE of 15.68% under a 500lx indoor LED light conditions [131]. Distinctly different from the above two scenarios, Tan et al. recently used two wide-bandgap donor materials (J52-F and PM7) and a A2-A1-D-A1-A2-structured acceptor BTA3 to construct ternary organic solar cells where PM7 acts as the third component, a satisfying PCE of 20.04% was gained under a 300 lux LED illumination owing to well-aligned energy level (Fig. 11a), matched spectrum, enhanced light absorption and the reduced E_{loss} in the ternary system [130] (see Fig. 12).

Apart from the ternary strategy, a suitable quaternary system can also be feasible. Recently, Ko and co-works utilized a PCDTBT:PTB7:PC₆₁BM:PC₇₁BM based quaternary BHJ which achieved the panchromatic absorption of indoor LED light and exhibited IQE values of nearly 100% [138]. Relevant parameters with various ratios are summarized in Table 1. The energy level in Fig. 11b means that the electron-transfer could occur from donors (PTB7 and PCDTBT) to acceptors (PC₆₁BM:PC₇₁BM), as well as from PTB7 to PCDTBT. This ensures an efficient charge-transport in the quaternary system. Attributed to the increased absorption window, superior charge transfer and extraction mechanism,

high shunt resistance, low series resistance and improved device stability compared to the controlled device, an optimal ratio of 5:5:3:12 realized the best PCE of 10.6% under a 500 lux LED illumination.

2.4. Trap state controlling strategy

Non-covalent molecular packed and solution processed organic semiconductors are inherently disordered materials. Structural imperfections and conformational defects (twists and kinks of polymer chains) could cause intrinsic disorder, while exposure to ambient environment can lead to extrinsic disorder. Both types of disorder would result in broadened electronic tails states, generating localized states in bandgap - trap states [139,140]. Device performance would be hampered as trap-states can induce trap-assisted recombination as well as non-radiative Shockley-Read-Hall recombination, giving rise to extra energy loss. Particularly, under weak indoor illuminations, the effects of trap-induced energy loss are amplified in such low charge carrier density conditions where the predominant bimolecular recombination under AM 1.5G irradiation becomes trivial [113,141,142]. Therefore, diminishing the trap-state density through optimized nanomorphology is significant for the enhanced device performance. Approaches such as optimizing the molecular configuration [143,144], improving the molecular packing [145,146], and regulating the vertical phase distribution are prone to be beneficial to reduce the trap-state density [147]. For IOPV devices, substantial endeavors have been devoted to the morphology optimization during fabrication process and the correct selection of photoactive materials to reduce the impact trap-induced recombination in recent years. The achievements are summarized as follows.

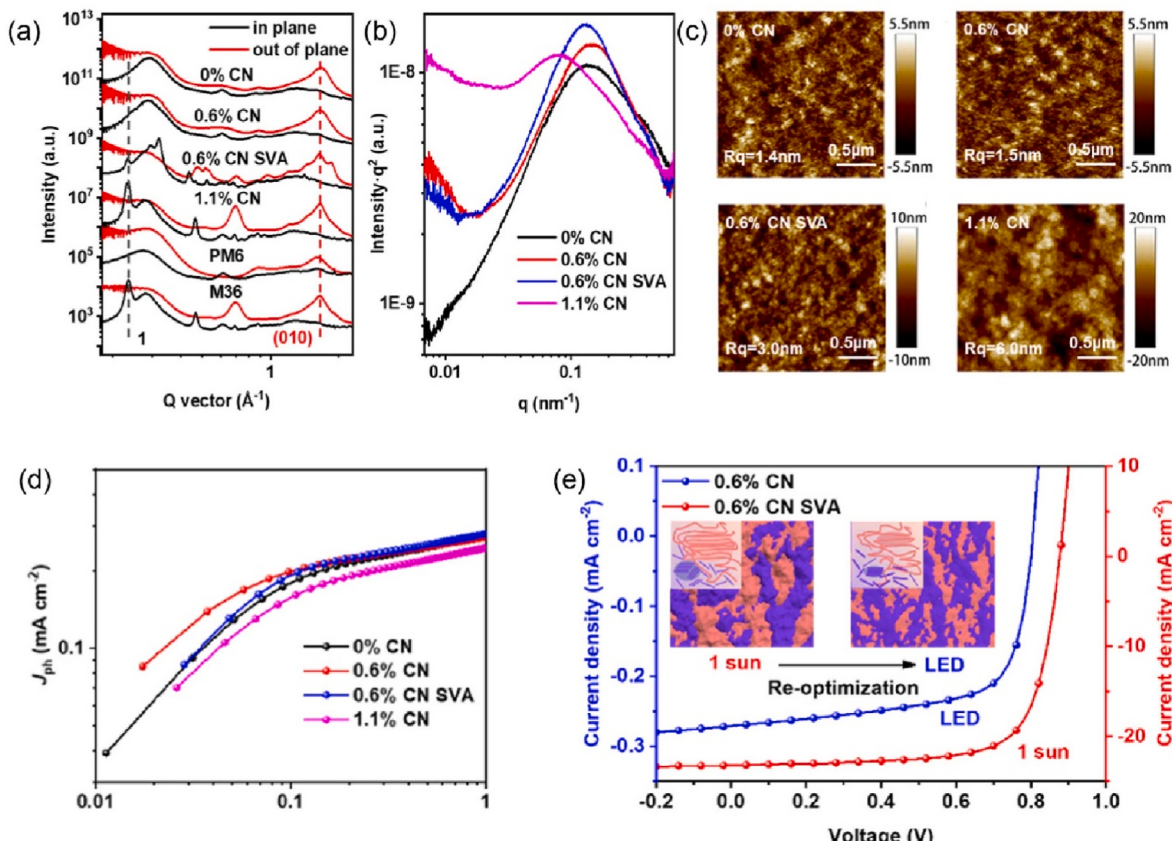


Fig. 14. (a) GIWAXS line profiles, (b) Resonant soft X-ray scattering (RSoXS) profiles of PM6 and M36 pure films and their blend films with SVA and various CN contents. (c) AFM height of PM6:M36 blend films prepared by different conditions. (d) J_{ph} as a function of effective applied voltage (V_{eff}) curves under 2000 lux LED illumination. (e) The J-V curves of BHJ under 1-sun and indoor conditions respectively. Reprinted with permission from ref. 148 (copyright The American Chemical Society 2021).

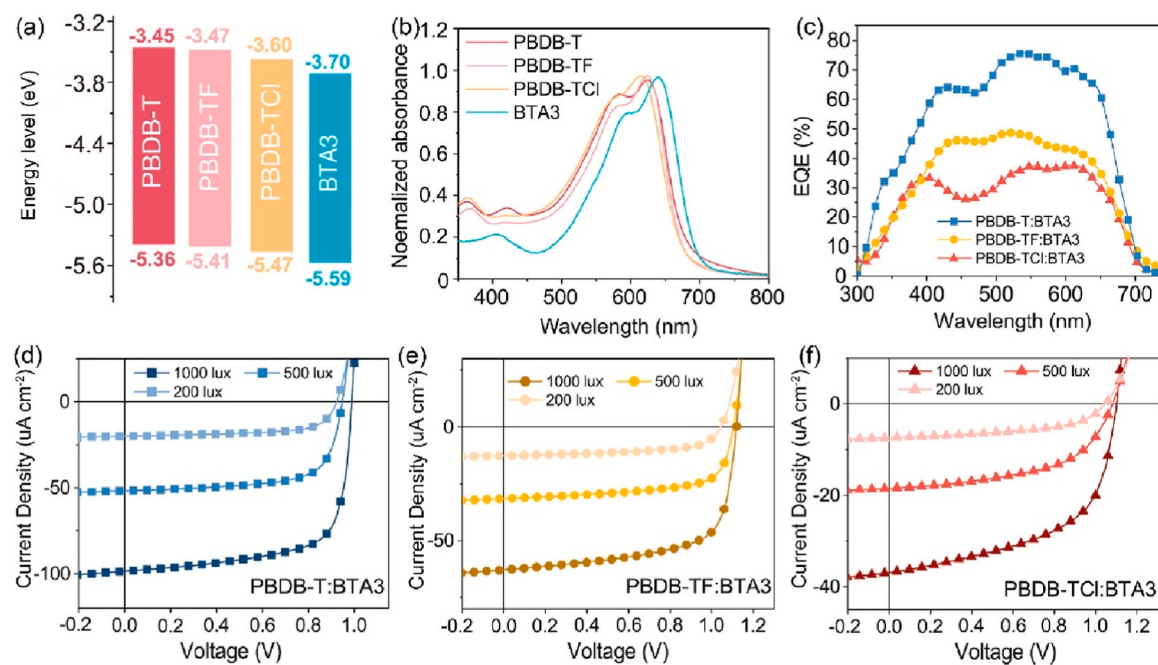


Fig. 15. (a) Energy levels of the materials. (b) Absorption spectra of PBDB-T, PBDB-TF, PBDB-TCI, and BTA3 neat films. (c) EQE spectra of the corresponding devices. (d) J–V curves of PBDB-T:BTAA3 devices under 2700 K LED with changing light intensity. (e) J–V curves of PBDB-TF:BTAA3 devices under 2700 K LED with changing light intensity. (f) J–V curves of PBDB-TCI:BTAA3 devices under 2700 K LED with changing light intensity. Reprinted with permission from ref. 149 (copyright The American Chemical Society 2021).

Based on PM6:M36 binary system, Ma and co-workers investigated the correlation between morphology and device performance by applying solvent vapor annealing (SVA) treatment and adding CN as the solvent additive [148]. Fig. 13a shows the absorbance of the corresponding films. In contrast to system with 0% CN content, the device containing 0.6% CN achieved the PCE value of 19.5% under a 2000 lux

illumination (Fig. 13b). The large fitted slope α of J_{sc} (Fig. 13c) as well as the smallest slope of $1.09 \frac{eV}{q}$ (Fig. 13d) in 0.6% CN condition imply the low bimolecular recombination losses and smallest Shockley-Read-Hall (SRH) recombination, which explains the better device performance in this condition. Grazing incidence wide-angle X-ray scattering (GIWAXS) and atomic force microscopy (AFM) were employed to analyze the

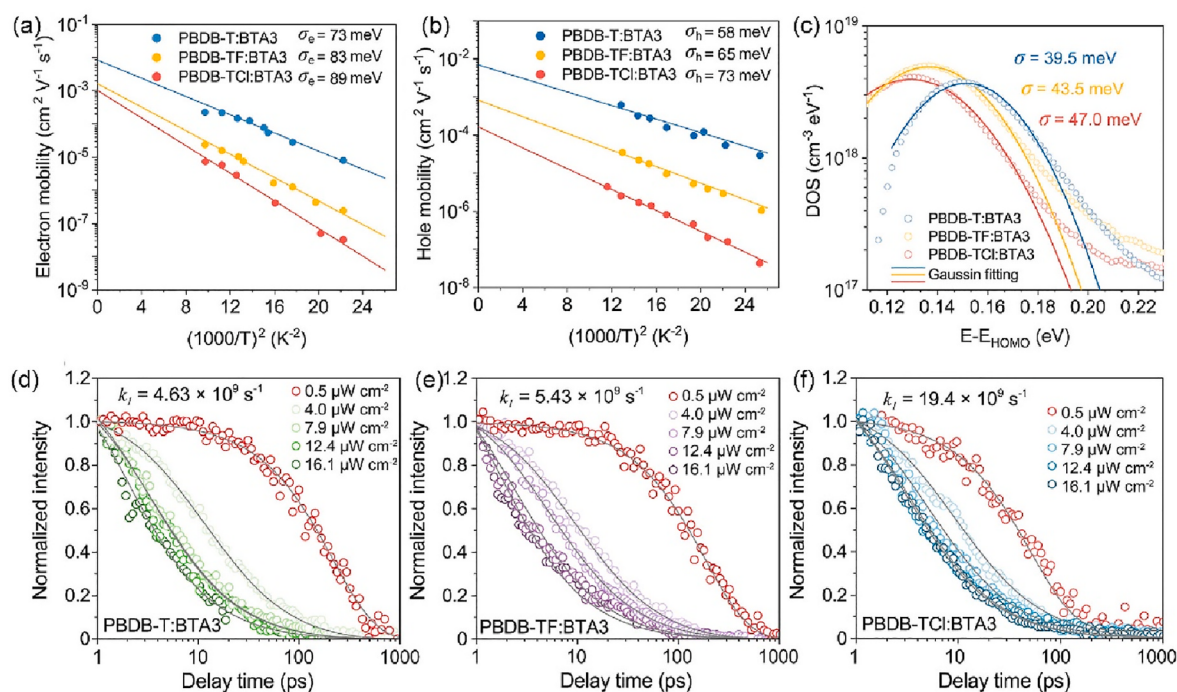


Fig. 16. (a) Zero-field electron mobility against $(1000/T)^2$ based on GDM fittings. (b) Zero-field hole mobility against $(1000/T)^2$ based on GDM fittings. (c) Defect DOS of the blending films and corresponding Gaussian fitting results. Pump-fluence dependent TA dynamics of: (d) PBDB-T:BTAA3, (e) PBDB-TF:BTAA3, and (f) PBDB-TCI:BTAA3 extracted at 1100 nm. Reprinted with permission from ref. 149 (copyright The American Chemical Society 2021).

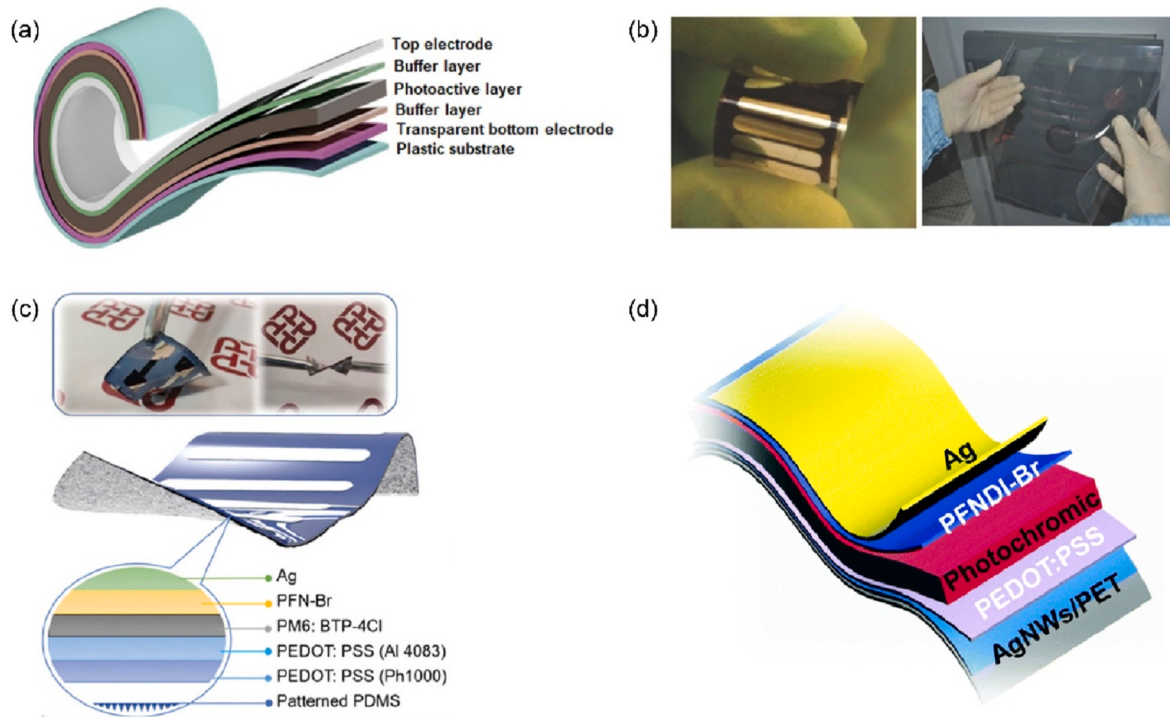


Fig. 17. (a) Typical device structure of flexible OSCs. Reprinted with permission from ref. 173 (copyright Springer Nature 2021) (b) Roll-to-roll-produced flexible transparent electrode. Reprinted with permission from ref. 191 (copyright John Wiley & Sons 2018) (c) PDMS substrate fabrication and corresponding device structure. Reprinted with permission from ref. 195 (copyright John Wiley & Sons 2021). (d) Device structure of the ternary organic solar cells for outdoor applications mentioned in this part. Reprinted with permission from ref. 193 (copyright John Wiley & Sons 2021).

microstructure and reveal the underlying physical process. Table 2 shows the results and corresponding structure parameters. It turns out that the coherence length of the film has increased originating from the improved d-spacing in terms of the system with 0.6% CN concentration which means enhanced crystalline. Besides, the AFM images displayed the increased root mean square (R_q) which implies improved crystalline when applying SVA treatment and increasing CN content (Fig. 14c). As shown in Fig. 14, both the system with 0.6% CN concentration have shown great domain purity (Fig. 14b and Table 2) but the system without SVA performed better under a 2000 lux LDE illumination (Fig. 14e) because of the lower dark current and better charge extraction ability (Fig. 14d). To conclude, the enhanced crystalline, improved phase separation, better domain purity as well as rather low R_q lead to optimized morphology contributing to the elevated performance indoor [144].

Hao and co-workers investigated the influence of trap effects by employing a series of PBDB-T based polymer donors (PBDB-T, PBDB-TF, PBDB-TCl) blending with BTA3 [149]. Photovoltaic performances of the above three system are quite different although the high V_{OC} and matched absorption acquired in systems (Fig. 15a and b). The decreasing trend in FF of the three different system with the reduction of the light intensity proved the influence of trap-induced recombination on device performance under low illumination conditions. Despite the lower V_{OC} value of PBDB-T:BTA3 system, its PCE significantly outperformed another two systems in all cases where the best obtained the PCE of 23.3% with the FF of 73.6% under a 1000 lux LED irradiation (Fig. 15d-f).

Markedly decrease of J_{sc} and FF explained the worse performance of these two systems. Subsequent characteristics such as transient absorption spectroscopy, energy loss and energy disorder solved the mystery. Transient absorption spectroscopy measurement indicated the charge carriers in PBDB-T:BTA3 are the least affected by the trap effects in weak illumination conditions (Fig. 16 d-f). Energy loss calculation displayed the smallest non-radiation energy loss in PBDB-T:BTA3 system

compared to other systems. Energy disorder measurement shows PBDB-T:BTA3 system possesses lowest hole energetic disorder (σ_h) and electron energetic disorder (σ_e) which implies PBDB-TF:BTA3 and PBDB-TCl:BTA3 have more broadened charge-transfer state tails that can work as trap states and thus induce the charge recombination (Fig. 16 a-c). Their work not only provides a detailed mechanism of the trap effect under indoor conditions, but offers a guideline on the correct selection of material designing for indoor applications.

Despite considerable strategies discussed above, it is far from enough compared with the achievements in AM 1.5G conditions. More efforts should be focused on the molecular design, nanomorphology of the films, and the device structure optimization to effectively reduce the trap-state densities and further elevated the overall IOPV device performance.

2.5. Interfacial engineering strategy

The interfacial topography between adjacent layers plays a critical role in multilayer devices and can affect the overall device performances. Particularly, interface features between photovoltaic layer and electrode are significantly essential for charge transportation and extraction. Therefore, electrode interlayers including hole transport layer (HTL) and electron transport layer (ETL) are commonly applied in the fabrication process as they can effectively reduce the contact energy barriers, enhance the built-in potential, and thereby promote the charge extraction process. Suitable selection of HTL and ETL materials are indispensable for the fabrication of high-performance IOPV devices. Herein, we summarized the recent endeavors of electrode interlayer innovations.

The HTL between the active layer and anode plays a crucial role in improving the performance of the OPV devices as it can promote the hole transport property, block the electron transport to the anode, reduce the hole recombination and lower the contacting barrier between the active layer and the anode [150]. PSS doped PEDOT, namely

PEDOT:PSS, is a commonly used HTL because of its high hole mobility and flexibility. However, its intrinsic properties such as sensitivity to humidity and high acidity drive the search of appropriate HTL materials for indoor OSCs [151,152]. Kim and co-workers synthesized the water-stable PANI with different doping (PSS) concentrations and use it as the HTL in the P3HT:ICBA system which achieved the PCE value of 8.1% [153] and 10% [154] under 500 lux and 1000 lux LED illuminations, respectively.

ETL is vital to reduce the work function of the cathode for effective electron injection and thus elevate the device efficiency. Both organic ETL and inorganic ETL are commonly applied in IPV devices. ZnO with high electron mobility and strong electrical conductivity is a widely used inorganic ETL material as it can effectively facilitate electron extraction by modifying the work function of cathode metals [155]. Nevertheless, inorganic ETL materials such as ZnO and LiF are difficult to form Ohmic contact with the active layer as the components of active layers are organic, and this incompatibility would limit the overall device performance. Moreover, vacuum-deposited ETL materials such as LiF and Ga are sensitive to ambient water and oxygen, and can further produce quenching site on the active layer or cathode surface, which are detrimental to carrier transport and extraction [156]. In contrast, organic ETLs which are easily to be modified through molecular design strategy are more suitable for OPV applications. Organic ETLs have higher electron affinity energy and can form excellent Ohmic contact with active layers. Various organic ETLs have been applied. Besides the commonly used organic ETLs such as PDINN and PDIN, PFN is frequently adopted as solution-processed electron transport layers in recent years. Estrada and coworkers fabricated the inverted organic solar cells based on p-DTS(FBTTh2)₂:PC₇₀BM BHJ films by using ZnO and PFN as ETLs under indoor warm white color light-emitting diode irradiation, respectively. The PCE reached 10.85% and maximum power density (MPP) of 45.1 μ W cm⁻² was obtained with PFN as ETL. Moreover, The PCE of the p-DTS(FBTTh2)₂:PC₇₀BM binary small molecular system using PFN or ZnO as ETL, maintained above 70% of the initial value after 1536 h of the indoor light illumination. Furthermore, Yan et al. team applied PDI-NO (a deep HOMO ETL material) to active layers and achieved a record PCE of 31% under 3000 K LED irradiation because of the suppressed leakage current and reduced trap-assisted recombination effects [157].

3. Multifunctional applications for IOPV devices

3.1. Flexibility

Wearable electronics such as smartwatch and medical sensor has incurred the seek for flexible and stretchable clean power sources. OSCs with the merits of light-weight, easy fabricating and flexibility are satisfactory candidates [158–164]. Collecting indoor ambient light by virtue of organic photovoltaics to drive these small portable electronics is exactly a judicious alternative.

Different from commonly used glass/ITO based rigid organic solar cells, flexible photovoltaics are fabricated from a flexible bottom transparent electrode on bendable plastic substrates [165–173]. And the typical device structure of flexible OSCs is shown in Fig. 17a. The plastic substrate and bottom transparent electrode are of utmost importance. Plastic substrates like polyethylene terephthalate (PET), poly-imides (PI), polydimethylsiloxane (PDMS) and perylene are commonly utilized substrates in flexible photovoltaics [174–177]. For electrode selection, searching for the electrode without deterioration after stretch is exactly suitable [178,179]. Tremendous efforts were made to find ITO alternative transparent electrodes. Among them, Ag nanowires, metal grid mesh, graphene and conducting polymers are appropriate ITO-free based transparent electrodes, which are widely applied in these fields [180–190]. Flexible bottom transparent electrode is required to combine the characteristics of high conductivity, high optical transmittance, high bending-resistance and low fabricating cost

synchronously just as displayed in Fig. 17b which meet the requirements of roll-to-roll production [191].

Despite PET and PI are commonly used plastic substrates [192], their intrinsic properties of relatively high Young's modulus indicate quite strong rigidness for them, and restrict their practical applications in flexible photovoltaics [193–195]. Lately, Li et al. employed the texturing stretchable substrate with low Young's modulus called PDMS to fabricate flexible photovoltaics for both outdoor and indoor conditions (Fig. 17c) [191], delivering a high PCE of 20.5% under indoor conditions and well light-direction tolerance which kept 38.5% of its initial PCE even at a relatively small incident angle of 10°. The PCE of the flexible device is nearly 2.5 times higher than that of the rigid device (ITO) at the extreme angle of incidence (80°). Therefore, under indoor conditions, the flexible device can obtain higher light utilization, which is significant for indoor light energy reuse and IOTs applications. For outdoor flexible photovoltaics, substantial achievements have been achieved. Sun and co-workers fabricated flexible organic solar cells based on PM6:BTP-eC9:ZY-4Cl with Ag NWs/PH1000 as bottom transparent electrode and gained the highest PCE for flexible photovoltaics while maintaining perfect bending resistance at the same time [189]. The corresponding device structure is displayed in Fig. 17d. Hou et al. employed an ultra-thin Ag transparent electrode and PCP-li interfacial layer based flexible photovoltaics on 50 nm PI substrate which outperformed excellent PCE of 15.56% for large-area (1 cm²) devices with superior bending stability [188]. Although huge achievements realized in laboratory, much efforts should be focus on the search for more efficient flexible substrates and the methods for large-scale production in order to realize the practical applications.

3.2. Semitransparency

The semi-transparent property of OSCs endows them with ample application prospects as they can be integrated into window, roof and indoor objects to generating electricity. In addition, by taking advantages of the excellent photon control and color variability ability of flexible polymer based one-dimensional photonic crystal, color control can be easily obtained, satisfying the color requirement for practical applications [196]. To be visually semi-transparent, the transmission light must have similar chromaticity with light source to preserve the naturally white property for the harmonious visual environment and comfort [197]. To this end, the chromaticity coordinates of the transmission light need to be close to that of the white light (0.33,0,0.33) according to the chromaticity diagram released by International Commission on Illumination (CIE) in 1931. To be physically semi-transparent, it often requires the photovoltaic has great transmittance in the visible region—the most sensitive human vision area. Equation (9) displaying the average visible transmittance (AVT) is deployed to calculate the averaged transmittance value of the semi-transparent photovoltaics in visible region on photonic response of the human eyes, in which $T(\lambda)$ is the transmittance spectrum of the semi-transparent photovoltaics, $V(\lambda)$ is the photopic response of human eyes and $S(\lambda)$ is spectrum of the light source. A high AVT value is the common pursuit for semi-transparent organic photovoltaics.

$$AVT = \frac{\int T(\lambda)V(\lambda)S(\lambda)d\lambda}{\int V(\lambda)S(\lambda)d\lambda} \quad (9)$$

Semi-transparent OPV devices have both indoor and outdoor applications. For semi-transparent OPV cells under the standard 1-Sun illumination, there are two general fabricating strategies: (i) decreasing the D:A ratios in the active layers to achieve highly transparent property; (ii) adopting narrow bandgap polymer donors and small molecular acceptors to utilize the near-infrared light while maintaining a high transmittance in visible light region [198–204]. Semi-transparent OPVs for outdoor applications have achieved great progress over the years in building-integrated photovoltaics as well as providing aesthetic comfort

Table 3

Parameters of semi-transparent organic solar cells under AM 1.5 G conditions.

Photoactive layer	HTL	ETL	V_{OC} [V]	J_{SC} [$\mu\text{A cm}^{-2}$]	FF [%]	PCE [%]	AVT (%)	ref
PTB7-Th: IEICO-4F	PEDOT: PSS	PDIN	0.709	18.8	67.8	9.1	27.1	[207]
D18: N3	PEDOT: PSS	PDIN	0.831	20.9	74.4	12.9	22.5	[208]
PM6:Y6	PEDOT: PSS	PDIN	0.852	20.4	71.4	12.4	18.6	[209]

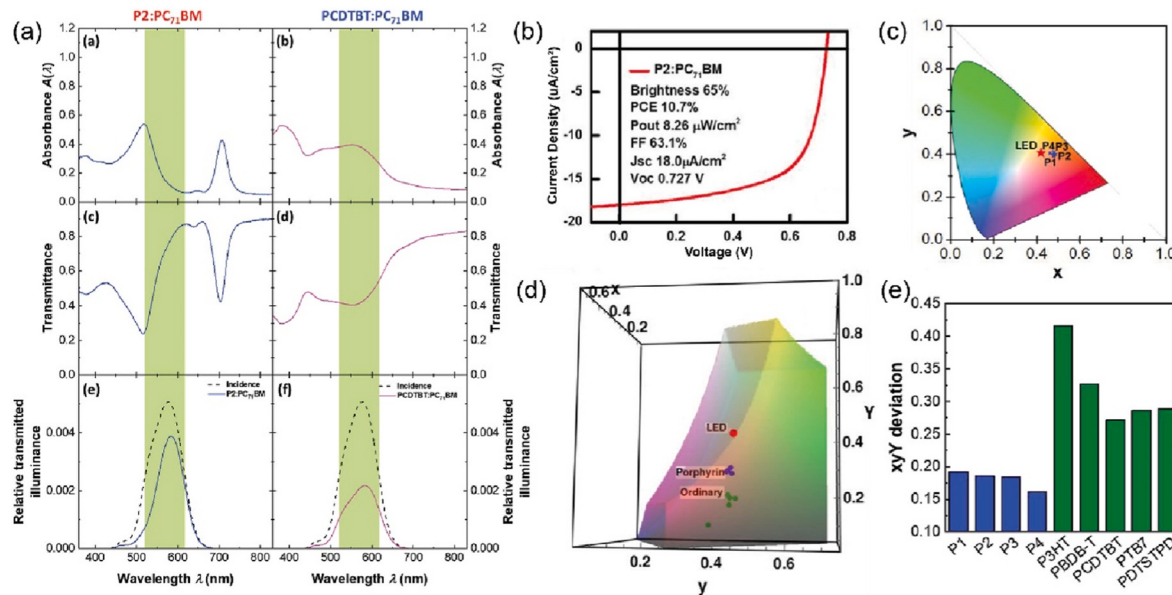


Fig. 18. (a) The spectral absorbance, transmittance transmitted illuminance relative to the incidence (black dashes) of P2:PC₇₁BM, a porphyrin-based BHJ absorber (left column) and PCDTBT:PC₇₁BM, an ordinary BHJ absorber (right column). (b) J–V curves of the P2:PC₇₁BM BHJ solar cell under a 300 lux LED irradiations. (c) The CIE (x, y) coordinates of the incident LED light (red star) and the light transmitted through the porphyrin:PC₇₁BM BHJ absorbers. (d) The CIE (x, y, Y) coordinates of the incident LED light (red) and the light transmitted through the porphyrin:PC₇₁BM BHJ absorbers (blue) and the ordinary OPV-donor:PC₇₁BM BHJ absorbers (green). (e) The x y Y deviation, defined as the distance between the BHJ and the incident LED light in (D), for different BHJs. Reprinted with permission from ref. 224 (copyright John Wiley & Sons 2020).

[116]. Zhang et al. used the narrow bandgap polymer donor PTB7-Th to fabricate semi-transparent OPVs by using diverse acceptors. When blending it with IEICO-4F (an ultra-narrow bandgap acceptor), an optimized PCE of 9.06% with 27.1% AVT was realized [205], and they further used it to fabricate ternary semi-transparent photovoltaic by adding a trace amount of IEICO-4F in PTB7-Th:COI8DFIC [206] and PTB7-Th:BDTTHIT-4F [207] binary system respectively, and achieved the PCE of 8.23% with 20.78 AVT and 9.40% with 24.6% AVT severally. Besides, the wide-bandgap donor D18 [208], the high performance photovoltaic system PM6:Y6 were also applied in semi-transparent photovoltaics frequently and the results are shown in Table 3 [209].

For indoor conditions, the semi-transparent photovoltaic devices exhibit a huge application prospect in indoor public places such as shopping mall, hospital and library [210–212]. Indoor environment exists less available NIR photons in contrast to outdoor conditions, so the fabrication strategies for indoor semi-transparent photovoltaics are to utilize indoor photons (400 nm–700 nm) as much as possible to achieve a relatively high PCE value and promise semi-transparent property at the same time [205,213–216]. With respect to materials for indoor semi-transparent applications, porphyrins and their derivatives are perfect candidates whatever as donors or acceptors [217–220]. Just as shown in Fig. 18a, their distinct weak absorption between Soret band and Q band (550 nm–700 nm) is conducive to make semi-transparent photovoltaics [215,221–223]. So and co-workers recently fabricated IPV of respectable PCE (>10%) (Fig. 18b) combined with relatively high transparency (>65%) based on P2 and PC₇₁BM [224], and the transmitted light through P2:PC₇₁BM has similar CIE color coordinates with the incident LED light source (Fig. 18c). Moreover, compared with the

Table 4
Parameters of the indoor semi-transparent photovoltaics.

Photoactive layer	V_{OC} [V]	J_{SC} [$\mu\text{A cm}^{-2}$]	FF [%]	PCE [%]	AVT (%)	CIE [x, y]	ref
C8TEBDT-2P:IDIC	0.590	24.6	62.5	12.3	70.0	(0.4185, 0.4049)	[126]
C8TBBDT-2P:IDIC	0.550	13.5	48.5	4.9	73.0	(0.4176, 0.4235)	[126]
P1:PC ₇₁ BM	0.581	21.9	49.4	8.2	63.0	(0.4810, 0.4108)	[224]
P2:PC ₇₁ BM	0.727	17.9	63.2	10.7	64.4	(0.4804, 0.3936)	[224]
P3:PC ₇₁ BM	0.682	16.8	58.6	8.7	65.1	(0.4864, 0.3989)	[224]
P4:PC ₇₁ BM	0.758	17.1	66.0	11.0	68.3	(0.4622, 0.4048)	[224]

ordinary absorbers, the porphyrin-based absorbers have CIE (x, y, Y) coordinates closer to the incident LED light (Fig. 18d) and possess smaller (x, y, Y) values (Fig. 18e), exhibiting huge potential working as semitransparent IPV and which could provide more similar visual perceptions and meanwhile can be applied in semitransparent IPVs. Simultaneously, they used two porphyrin dimers (C8TEBDT-2P and C8TBBDT-2P) as donors with IDIC as acceptors for semi-transparent IPV, and consequently both the above two systems exhibit pronounced transparency over 70% with eminent PCE values under 300 lux LED irradiations. Their work further verified the feasibility of porphyrin donors for high-transparent indoor photovoltaics (see Table 4).

4. Outlooks

IOPVs devices deliver abroad prospect in terms of powering small off-grid devices connected to the internet and exactly are the best candidate for the indoor photovoltaic market. We summarized the different strategies to improve the device performance in recent years elaborately and illustrate their applications in flexible and semi-transparent photovoltaic devices. Despite IOPV device has achieved the PCE of up to 30% with excellent stability currently because of the invent of novel non-fullerene acceptors through molecular designing. A huge gap between the theoretical PCE limitations ($\approx 60\%$) and experimental results still exist and the PCE exhibits huge elevating potentials. For the further surge of the efficiency, more efforts ought to be focus on the wide-bandgap material design and mediated trap-assisted recombination, as well as alleviated energy losses. Meanwhile, compared to the standard 1-Sun assessment methods, a universal PCE measurement protocol under indoor conditions has not been established yet, so the testing accuracy of the device performance is doubtful. Hence, a standard measurement agreement is urgent for IOPVs cells for the reliable device performance assessment. For the large-scale device fabrication, processing methods such as slot-die and blade coating should be considered, non-halogen solvents are supposed to replace the commonly used chloroform and chlorobenzene to meet the green production requirements. Finally, future exploration is required to pay more attention to more cost-effective, practical flexible substrate and semi-transparent electrode for the fabrication of flexible and semi-transparent photovoltaics respectively to better benefiting the internet of things.

Declaration of competing interest

The authors declare that they have no known competing financial interests or personal relationships that could have appeared to influence the work reported in this paper.

Data availability

Data will be made available on request.

Acknowledgements

This work was supported by the Shandong Provincial Natural Science Foundation (ZR202102220369), Major Program of Natural Science Foundation of Shandong Province (ZR2019ZD43), Natural Science Foundation of China (52073162), and the Qilu Young Scholar Program of Shandong University. The authors acknowledge the National Natural Science Foundation of China (52073207) for financial support.

References

- [1] K.Z.A. Awan, A B energy, Renew. Sustain. Energy Rev. 33 (2014) 236.
- [2] W. Dong, et al., Engineering the defects and microstructures in ferroelectrics for enhanced/novel properties: an emerging way to cope with energy crisis and environmental pollution, Adv. Sci. 9 (13) (2022), 2105368.
- [3] S.C. Peter, Reduction of CO₂ to chemicals and fuels: a solution to global warming and energy crisis, ACS Energy Lett. 3 (7) (2018) 1557–1561.
- [4] Z. Yin, et al., A comprehensive review on cultivation and harvesting of microalgae for biodiesel production: environmental pollution control and future directions, Bioresour. Technol. 301 (2020), 122804.
- [5] H. Kang, et al., Bulk-heterojunction organic solar cells: five core technologies for their commercialization, Adv. Mater. 28 (36) (2016) 7821–7861.
- [6] Y. Chang, et al., Progress and prospects of thick-film organic solar cells, J. Mater. Chem. 9 (6) (2021) 3125–3150.
- [7] X.M. Li, et al., Recent progress of benzodifuran-based polymer donors for high-performance organic photovoltaics, Small Sci 2 (6) (2022), 2200006.
- [8] X. Wang, et al., Recent progress of organic photovoltaics with efficiency over 17%, Energies 14 (14) (2021) 4200.
- [9] C. Xu, et al., Recent progress in all-small-molecule organic photovoltaics, J. Mater. Chem. 10 (12) (2022) 6291–6329.
- [10] B. Bose, Global warming: energy, environmental pollution, and the impact of power electronics, IEEE Ind. Electron. Mag. 4 (1) (2010) 6–17.
- [11] R. Søndergaard, et al., Roll-to-roll fabrication of polymer solar cells, Mater. Today 15 (1–2) (2012) 36–49.
- [12] L. Xie, et al., Recent progress of organic photovoltaics for indoor energy harvesting, Nano Energy 82 (2021), 105770.
- [13] T.A. Gessert, T.J. Coutts, Requirements of electrical contacts to photovoltaic solar cells, Mrs Proceedings 181 (1990) 237–246.
- [14] P. Bi, et al., Progress in organic solar cells: materials, physics and device engineering, Chin. J. Chem. 39 (9) (2021) 2607–2625.
- [15] H. Hoppe, N.S. Sariciftci, Organic solar cells: an overview, J. Mater. Res. 19 (7) (2011) 1924–1945.
- [16] J. Hou, et al., Organic solar cells based on non-fullerene acceptors, Nat. Mater. 17 (2) (2018) 119–128.
- [17] Y. Liu, et al., Recent progress in organic solar cells (Part I material science), Sci. China Chem. 65 (2) (2021) 224–268.
- [18] B. Xiao, et al., Relationship between fill factor and light intensity in solar cells based on organic disordered semiconductors: the role of tail states, Phys. Rev. Appl. 14 (2) (2020), 024034.
- [19] K.N. Zhang, et al., Reducing limitations of aggregation-induced photocarrier trapping for photovoltaic stability via tailoring intermolecular electron–phonon coupling in highly efficient quaternary polymer solar cells, Adv. Energy Mater. 12 (6) (2021), 2103371.
- [20] K. Jin, et al., 18.69% PCE from organic solar cells, J. Semiconduc. 42 (6) (2021), 060502.
- [21] K. Jin, et al., D18, an eximious solar polymer, J. Semiconduc. 42 (1) (2021), 010502.
- [22] J. Qin, et al., A chlorinated copolymer donor demonstrates a 18.13% power conversion efficiency, J. Semiconduc. 42 (1) (2021), 010501.
- [23] J. Wang, et al., Structural regulation of thiophene-fused benzotriazole as a “π-bridge” for A-π-D-π-A type acceptor:P3HT-based OSCs to achieve high efficiency, J. Phys. Chem. C 9 (10) (2021) 6520–6528.
- [24] L. Ma, et al., Completely non-fused electron acceptor with 3D-interpenetrated crystalline structure enables efficient and stable organic solar cell, Nat. Commun. 12 (1) (2021) 5093.
- [25] S. Qin, et al., Molecular properties and aggregation behavior of small-molecule acceptors calculated by molecular simulation, ACS Omega 6 (22) (2021) 14467–14475.
- [26] C. Sun, et al., Quinoxaline-based D-A copolymers for the applications as polymer donor and hole transport material in polymer/perovskite solar cells, Adv. Mater. 20 (2021), 2104161.
- [27] J. Wang, et al., An asymmetric wide-bandgap acceptor simultaneously enabling highly efficient single-junction and tandem organic solar cells, Energy Environ. Sci. 15 (4) (2022) 1585–1593.
- [28] C. Yang, et al., Low-cost and efficient organic solar cells based on polythiophene- and poly(thiophene vinylene)-related donors, Aggregate 8 (2021) 111.
- [29] H. Yang, et al., Effects of heteroatom substitution on the photovoltaic performance of donor materials in organic solar cells, Acc. Mater. Res. 2 (11) (2021) 986–997.
- [30] B. Zheng, et al., Conjugated mesopolymer achieving 15% efficiency single-junction organic solar cells, Adv. Sci. 9 (8) (2022), 2105430.
- [31] C. Zhu, et al., A quinoxaline-based D-A copolymer donor achieving 17.62% efficiency of organic solar cells, Adv. Mater. 33 (23) (2021), 2100474.
- [32] X. Li, et al., Benzo[1,2-b:4,5-b']difuran based polymer donor for high-efficiency (>16%) and stable organic solar cells, Adv. Energy Mater. 12 (9) (2022), 2103684.
- [33] H. Lu, et al., High-efficiency organic solar cells based on asymmetric acceptors bearing one 3D shape-persistent terminal group, Adv. Funct. Mater. 31 (35) (2021), 2103445.
- [34] H. Wang, et al., Chlorination enabling a low-cost benzodithiophene-based wide-bandgap donor polymer with an efficiency of over 17%, Adv. Mater. 34 (4) (2022), 2105483.
- [35] Z. Zhang, et al., Nonfullerene acceptors comprising a naphthalene core for high efficiency organic solar cells, RSC Adv. 9 (67) (2019) 39163–39169.
- [36] W. Gao, et al., Asymmetric acceptors enabling organic solar cells to achieve an over 17% efficiency: conformation effects on regulating molecular properties and suppressing nonradiative energy loss, Adv. Energy Mater. 11 (4) (2020), 2003177.
- [37] Y. Ji, et al., Synergistic effect of incorporating intra- and inter-molecular charge transfer in nonfullerene acceptor molecules for highly-efficient organic solar cells, J. Mater. Chem. 9 (31) (2021) 16834–16840.
- [38] T. Xia, et al., Efficient fused-ring extension of A-D-A-type non-fullerene acceptors by a symmetric replicating core unit strategy, Chemistry 26 (54) (2020) 12411–12417.
- [39] H. Yu, et al., Regio-regular polymer acceptors enabled by determined fluorination on end groups for all-polymer solar cells with 15.2 % efficiency, Angew. Chem., Int. Ed. Engl. 60 (18) (2021) 10137–10146.
- [40] A. Zeng, et al., A chlorinated donor polymer achieving high-performance organic solar cells with a wide range of polymer molecular weight, Adv. Funct. Mater. 31 (33) (2021), 2102413.
- [41] M. Zhang, et al., Metallated terpolymer donors with strongly absorbing iridium complex enables polymer solar cells with 16.71% efficiency, Chem. Eng. J. 430 (2022), 132832.
- [42] S. Bao, et al., Volatilizable solid additive-assisted treatment enables organic solar cells with efficiency over 18.8% and fill factor exceeding 80, Adv. Mater. 33 (48) (2021), 2105301.

- [43] X. Ma, et al., Achieving 17.4% efficiency of ternary organic photovoltaics with two well-compatible nonfullerene acceptors for minimizing energy loss, *Adv. Energy Mater.* 10 (2020), 2001404.
- [44] M. Nam, et al., All-Day operating quaternary blend organic photovoltaics, *Adv. Funct. Mater.* 29 (16) (2019), 1900154.
- [45] Y. Zeng, et al., Exploring the charge dynamics and energy loss in ternary organic solar cells with a fill factor exceeding 80%, *Adv. Energy Mater.* 11 (31) (2021), 2101338.
- [46] M.A. Adil, et al., Unconventional third components for ternary organic solar cells, *Mater. Today Energy* 21 (2021).
- [47] M.A. Adil, et al., Utilizing ternary strategy to reduce the influence of polymer batch-to-batch variation in organic solar cells, *Sol. RRL* 6 (6) (2022).
- [48] Y. Cai, et al., A well-mixed phase formed by two compatible non-fullerene acceptors enables ternary organic solar cells with efficiency over 18.6, *Adv. Mater.* 33 (33) (2021), 2101733.
- [49] P. Bi, et al., Dual Förster resonance energy transfer effects in non-fullerene ternary organic solar cells with the third component embedded in the donor and acceptor, *J. Mater. Chem. 5* (24) (2017) 12120–12130.
- [50] K. Feng, et al., Highly efficient ternary all-polymer solar cells with enhanced stability, *Adv. Funct. Mater.* 31 (5) (2020), 2008494.
- [51] Y. Wang, et al., Organic photovoltaics with 300 nm thick ternary active layers exhibiting 15.6% efficiency, *J. Mater. Chem. C* 9 (31) (2021) 9892–9898.
- [52] W. Xu, et al., Smart ternary strategy in promoting the performance of polymer solar cells based on bulk-heterojunction or layer-by-layer structure, *Small* 18 (4) (2022), 2104215.
- [53] J. Du, et al., Polymerized small molecular acceptor based all-polymer solar cells with an efficiency of 16.16% via tuning polymer blend morphology by molecular design, *Nat. Commun.* 12 (1) (2021) 5264.
- [54] H. Fan, et al., Anthracene-assisted morphology optimization in photoactive layer for high-efficiency polymer solar cells, *Adv. Funct. Mater.* 31 (37) (2021), 2103944.
- [55] M. Gao, et al., Control of aggregated structure of photovoltaic polymers for high-efficiency solar cells, *Aggregate* 2 (5) (2021) 46.
- [56] R. Yu, et al., Quadrupole moment induced morphology control via a highly volatile small molecule in efficient organic solar cells, *Adv. Funct. Mater.* 31 (18) (2021), 2010535.
- [57] G. Cai, et al., Pushing the efficiency of high open-circuit voltage binary organic solar cells by vertical morphology tuning, *Adv. Sci.* (2022), 2200578.
- [58] Y. Cai, et al., Vertically optimized phase separation with improved exciton diffusion enables efficient organic solar cells with thick active layers, *Nat. Commun.* 13 (1) (2022) 2369.
- [59] K. Weng, et al., Optimized active layer morphology toward efficient and polymer batch insensitive organic solar cells, *Nat. Commun.* 11 (1) (2020) 2855.
- [60] L. Ye, et al., Unraveling the influence of non-fullerene acceptor molecular packing on photovoltaic performance of organic solar cells, *Nat. Commun.* 11 (1) (2020) 6005.
- [61] L. Zhang, et al., High miscibility compatible with ordered molecular packing enables an excellent efficiency of 16.2% in all-small-molecule organic solar cells, *Adv. Mater.* 34 (5) (2022), 2106316.
- [62] F. Zhao, et al., Modulating morphology via side-chain engineering of fused ring electron acceptors for high performance organic solar cells, *Sci. China Chem.* 62 (6) (2019) 790–796.
- [63] R. Zhou, et al., All-small-molecule organic solar cells with over 14% efficiency by optimizing hierarchical morphologies, *Nat. Commun.* 10 (1) (2019) 5393.
- [64] W. Gao, et al., Asymmetric isomer effects in benzofc]1,2,5]thiadiazole-Fused nonacyclic acceptors: dielectric constant and molecular crystallinity control for significant photovoltaic performance enhancement, *Adv. Funct. Mater.* 31 (2021), 2104369.
- [65] K. Zhang, et al., High-performance ternary organic solar cells with morphology-modulated hole transfer and improved ultraviolet photostability, *Sol. RRL* 4 (7) (2020), 2000165.
- [66] Y. Cui, et al., Single-junction organic photovoltaic cell with 19% efficiency, *Adv. Mater.* 33 (41) (2021), 2102420.
- [67] Y. Xie, et al., High-efficiency organic solar cells enabled by an alcohol-washable solid additive, *Sci. China Chem.* 64 (12) (2021) 2161–2168.
- [68] W. Yang, et al., Simultaneous enhanced efficiency and thermal stability in organic solar cells from a polymer acceptor additive, *Nat. Commun.* 11 (1) (2020) 1218.
- [69] R. Yu, et al., Realization of high performance for PM6:Y6 based organic photovoltaic cells, *J. Energy Chem.* 61 (2021) 29–46.
- [70] J. Yao, et al., Perylene-diimide-based cathode interlayer materials for high performance organic solar cells, *SusMat* 2 (2022) 1–21.
- [71] R. Yu, et al., Efficient interface modification via multi-site coordination for improved efficiency and stability in organic solar cells, *Energy Environ. Sci.* 15 (2) (2022) 822–829.
- [72] C. Chen, et al., A novel, weakly N-doped cathode-modifying layer in organic solar cells, *Energy Technol.* 9 (8) (2021), 2100281.
- [73] Z. Zhang, et al., Polymerized small-molecule acceptor as an interface modulator to increase the performance of all-small-molecule solar cells, *Adv. Energy Mater.* 12 (3) (2021), 2102394.
- [74] J. Qiao, et al., Manipulating the interlayer carrier diffusion and extraction process in organic-inorganic heterojunctions: from 2D to 3D structures, *npj 2D Mater. Appl.* 6 (1) (2022), 00278.
- [75] R. Sun, et al., Single-junction organic solar cells with 19.17% efficiency enabled by introducing one asymmetric guest acceptor, *Adv. Mater.* (2022), 2110147.
- [76] Z. Zheng, et al., Tandem organic solar cell with 20.2% efficiency, *Joule* 6 (1) (2022) 171–184.
- [77] T. Zhang, et al., A universal nonhalogenated polymer donor for high-performance organic photovoltaic cells, *Adv. Mater.* 34 (2) (2022), 2105803.
- [78] Y. Zhang, et al., Indoor organic photovoltaics, *Sci. Bull.* 65 (24) (2020) 2040–2042.
- [79] F.-C. Chen, Emerging organic and organic/inorganic hybrid photovoltaic devices for specialty applications: low-level-lighting energy conversion and biomedical treatment, *Adv. Opt. Mater.* 7 (1) (2019).
- [80] N.-W. Teng, et al., Plasmonic-enhanced organic photovoltaic devices for low-power light applications, *IEEE J. Photovoltaics* 8 (3) (2018) 752–756.
- [81] C.-L. Huang, et al., Plasmonic effects of copper nanoparticles in polymer photovoltaic devices for outdoor and indoor applications, *Appl. Phys. Lett.* 116 (25) (2020).
- [82] J.K.W. Ho, et al., From 33% to 57% – an elevated potential of efficiency limit for indoor photovoltaics, *J. Mater. Chem. 8* (4) (2020) 1717–1723.
- [83] B. Du, et al., Nondestructive inspection, testing and evaluation for Si-based, thin film and multi-junction solar cells: an overview, *Renew. Sustain. Energy Rev.* 78 (2017) 1117–1151.
- [84] K. Sharma, et al., Dye-sensitized solar cells: fundamentals and current status, *Nanoscale Res. Lett.* 13 (1) (2018) 381.
- [85] B.T. Muhammad, et al., Halide perovskite-based indoor photovoltaics: recent development and challenges, *Mater. Today Energy* 23 (2022), 100907.
- [86] M.H. Kao, et al., Low-temperature growth of hydrogenated amorphous silicon carbide solar cell by inductively coupled plasma deposition toward high conversion efficiency in indoor lighting, *Sci. Rep.* 7 (1) (2017), 12706.
- [87] Y. Cao, et al., Direct contact of selective charge extraction layers enables high-efficiency molecular photovoltaics, *Joule* 2 (6) (2018) 1108–1117.
- [88] M. Li, et al., Interface modification by ionic liquid: a promising candidate for indoor light harvesting and stability improvement of planar perovskite solar cells, *Adv. Energy Mater.* 8 (24) (2018), 1801509.
- [89] B.P. Lechene, et al., Organic solar cells and fully printed super-capacitors optimized for indoor light energy harvesting, *Nano Energy* 26 (2016) 631–640.
- [90] M. Mainville, M. Leclerc, Recent progress on indoor organic photovoltaics: from molecular design to production scale, *ACS Energy Lett.* 5 (4) (2020) 1186–1197.
- [91] T. Wang, et al., One-micron-thick organic indoor light harvesters with low photocurrent loss and fill factors over 67%, *J. Mater. Chem. 9* (23) (2021) 13515–13521.
- [92] J. Cao, et al., Star polymer donors, *J. Semiconduct.* 43 (7) (2022).
- [93] E. Feng, et al., 26.75 cm² organic solar modules demonstrate a certified efficiency of 14.34%, *J. Semiconduct.* 43 (10) (2022).
- [94] G. Dennerl, et al., A self-rechargeable and flexible polymer solar battery, *Sol. Energy* 81 (8) (2007) 947–957.
- [95] I. Mathews, et al., Technology and market perspective for indoor photovoltaic cells, *Joule* 3 (6) (2019) 1415–1426.
- [96] J.-L. Wu, et al., Near-infrared laser-driven polymer photovoltaic devices and their biomedical applications, *Energy Environ. Sci.* 4 (9) (2011) 3374.
- [97] S.-S. Yang, et al., Toward high-performance polymer photovoltaic devices for low-power indoor applications, *Sol. RRL* 1 (12) (2017), 1700174.
- [98] A. Venkateswararao, et al., Device characteristics and material developments of indoor photovoltaic devices, *Mater. Sci. Eng., A R* 139 (2020), 100517.
- [99] X. Hou, et al., Indoor application of emerging photovoltaics—progress, challenges and perspectives, *J. Mater. Chem. 8* (41) (2020) 21503–21525.
- [100] H.S. Ryu, et al., Recent progress in indoor organic photovoltaics, *Nanoscale* 12 (10) (2020) 5792–5804.
- [101] X. Xu, et al., Recent advances in wide bandgap polymer donors and their applications in organic solar cells, *Chin. J. Chem.* 39 (2) (2021) 243–254.
- [102] D. Venkataraman, Cutting, Indoor light recycling a new home for organic, *J. Phys. Chem. C* 16 (2016) 10367–10370.
- [103] H.K.H. Lee, et al., Organic photovoltaic cells – promising indoor light harvesters for self-sustainable electronics, *J. Mater. Chem. 6* (14) (2018) 5618–5626.
- [104] H. Yin, et al., Designing a ternary photovoltaic cell for indoor light harvesting with a power conversion efficiency exceeding 20%, *J. Mater. Chem. 6* (18) (2018) 8579–8585.
- [105] H.K.H. Lee, et al., Is organic photovoltaics promising for indoor applications? *Appl. Phys. Lett.* 108 (25) (2016), 253301.
- [106] C. Li, et al., Non-fullerene acceptors with branched side chains and improved molecular packing to exceed 18% efficiency in organic solar cells, *Nat. Energy* 6 (6) (2021) 605–613.
- [107] J. Zhang, et al., Chlorinated thiophene end groups for highly crystalline alkylated non-fullerene acceptors toward efficient organic solar cells, *Chem. Mater.* 31 (17) (2019) 6672–6676.
- [108] M.A. Saeed, et al., Indoor organic photovoltaics: optimal cell design principles with synergistic parasitic resistance and optical modulation effect, *Adv. Energy Mater.* 11 (27) (2021), 2003103.
- [109] A. Shankar, et al., Techno-economic and energy assessment of building integrated photovoltaic module as an envelope of the building, *Int. Trans. Electr. Energy Syst.* 31 (11) (2021), 13105.
- [110] Z.-H. Chen, et al., Chromaticity manipulation of indoor photovoltaic cells, *Appl. Phys. Lett.* 118 (4) (2021), 043301.
- [111] S. Zhang, et al., Over 14% efficiency in polymer solar cells enabled by a chlorinated polymer donor, *Adv. Mater.* 30 (20) (2018), 1800868.
- [112] A. Al-Fuqaha, et al., Internet of things: a survey on enabling technologies, protocols, and applications, *IEEE Commun. Surv. Tutorials* 17 (4) (2015) 2347–2376.
- [113] C.M. Proctor, T.-Q. Nguyen, Effect of leakage current and shunt resistance on the light intensity dependence of organic solar cells, *Appl. Phys. Lett.* 106 (8) (2015), 083301.

- [114] Y. Xu, et al., Organic photovoltaic cells with high efficiencies for both indoor and outdoor applications, *Mater. Chem. Front.* 5 (2) (2021) 893–900.
- [115] Y. Cui, et al., 1 cm² organic photovoltaic cells for indoor application with over 20% efficiency, *Adv. Mater.* 31 (42) (2019), 1904512.
- [116] Y. Cui, et al., Wide-gap non-fullerene acceptor enabling high-performance organic photovoltaic cells for indoor applications, *Nat. Energy* 4 (9) (2019) 768–775.
- [117] P. Bi, et al., A high-performance nonfused wide-bandgap acceptor for versatile photovoltaic applications, *Adv. Mater.* 34 (5) (2022), 2108090.
- [118] F. Bai, et al., A highly crystalline non-fullerene acceptor enabling efficient indoor organic photovoltaics with high EQE and fill factor, *Joule* 5 (5) (2021) 1231–1245.
- [119] X. Li, et al., Medium band-gap non-fullerene acceptors based on a benzothiophene donor moiety enabling high-performance indoor organic photovoltaics, *Energy Environ. Sci.* 14 (8) (2021) 4555–4563.
- [120] Z. Ding, et al., All-polymer indoor photovoltaics with high open-circuit voltage, *J. Mater. Chem. T* (46) (2019) 26533–26539.
- [121] S. Park, et al., High-performance and stable nonfullerene acceptor-based organic solar cells for indoor to outdoor light, *ACS Energy Lett.* 5 (1) (2019) 170–179.
- [122] H.I. Je, et al., Understanding the performance of organic photovoltaics under indoor and outdoor conditions: effects of chlorination of donor polymers, *ACS Appl. Mater. Interfaces* 12 (20) (2020) 23181–23189.
- [123] R. Singh, et al., Highly efficient indoor organic solar cells by voltage loss minimization through fine-tuning of polymer structures, *ACS Appl. Mater. Interfaces* 11 (40) (2019) 36905–36916.
- [124] Y.J. You, et al., Highly efficient indoor organic photovoltaics with spectrally matched fluorinated phenylene-alkoxybenzothiadiazole-based wide bandgap polymers, *Adv. Funct. Mater.* 29 (27) (2019) 1901171.
- [125] Z. Yang, et al., High-performance indoor organic solar cells based on a double-cable conjugated polymer, *Sol. RRL* (2022), 2100981.
- [126] V. Piradi, et al., Highly semitransparent indoor nonfullerene organic solar cells based on benzodithiophene-bridged porphyrin dimers, *Energy Technol.* 10 (2) (2021), 2100908.
- [127] Y. Cui, et al., Accurate photovoltaic measurement of organic cells for indoor applications, *Joule* 5 (5) (2021) 1016–1023.
- [128] S.V. Dayneko, et al., Indoor photovoltaics: photoactive material selection, greener ink formulations, and slot-die coated active layers, *ACS Appl. Mater. Interfaces* 11 (49) (2019) 46017–46025.
- [129] C.-Y. Liao, et al., Processing strategies for an organic photovoltaic module with over 10% efficiency, *Joule* 4 (1) (2020) 189–206.
- [130] Y. Cui, et al., Organic photovoltaic cells for indoor applications: opportunities and challenges, *ACS Appl. Mater. Interfaces* 12 (35) (2020) 38815–38828.
- [131] P. Bi, X. Hao, Versatile ternary approach for novel organic solar cells: a review, *Sol. RRL* 3 (1) (2019), 1800263.
- [132] P. Cheng, X. Zhan, Stability of organic solar cells: challenges and strategies, *Chem. Soc. Rev.* 45 (9) (2016) 2544–2582.
- [133] Y. Bai, et al., Ternary blend strategy in benzotriazole-based organic photovoltaics for indoor application, *Green Energy Environ.* 6 (6) (2021) 920–928.
- [134] R. Singh, et al., Ternary blend strategy for achieving high-efficiency organic photovoltaic devices for indoor applications, *Chemistry* 25 (24) (2019) 6154–6161.
- [135] J. Yuan, et al., Single-junction organic solar cell with over 15% efficiency using fused-ring acceptor with electron-deficient core, *Joule* 3 (4) (2019) 1140–1151.
- [136] J. Cao, et al., The origin and evolution of Y6 structure, *J. Semiconduct.* 43 (3) (2022).
- [137] Y. Cho, et al., Guest-oriented non-fullerene acceptors for ternary organic solar cells with over 16.0% and 22.7% efficiencies under one-sun and indoor light, *Nano Energy* 75 (2020), 104896.
- [138] S. Shin, et al., Quaternary indoor organic photovoltaic device demonstrating panchromatic absorption and power conversion efficiency of 10%, *Dyes Pigments* 163 (2019) 48–54.
- [139] Y. Zhang, et al., An electron acceptor analogue for lowering trap density in organic solar cells, *Adv. Mater.* 33 (14) (2021), 2008134.
- [140] G. Zuo, et al., General rule for the energy of water-induced traps in organic semiconductors, *Nat. Mater.* 18 (6) (2019) 588–593.
- [141] H.F. Haneef, et al., Charge carrier traps in organic semiconductors: a review on the underlying physics and impact on electronic devices, *J. Mater. Chem. C* 8 (3) (2020) 759–787.
- [142] C.M. Proctor, et al., Nongeminate recombination and charge transport limitations in diketopyrrolopyrrole-based solution-processed small molecule solar cells, *Adv. Funct. Mater.* 23 (28) (2013) 3584–3594.
- [143] M. Shi, et al., Remove the water-induced traps toward improved performance in organic solar cells, *Sci. China Mater.* 64 (11) (2021) 2629–2644.
- [144] J. Wu, et al., Exceptionally low charge trapping enables highly efficient organic bulk heterojunction solar cells, *Energy Environ. Sci.* 13 (8) (2020) 2422–2430.
- [145] L. Ma, et al., High-efficiency nonfullerene organic solar cells enabled by 1000 nm thick active layers with a low trap-state density, *ACS Appl. Mater. Interfaces* 12 (16) (2020) 18777–18784.
- [146] Y. Xia, et al., Molecular doping inhibits charge trapping in low-temperature-processed ZnO toward flexible organic solar cells, *ACS Appl. Mater. Interfaces* 13 (12) (2021) 14423–14432.
- [147] P. Bi, et al., Suppressing trap states and energy loss by optimizing vertical phase distribution through ternary strategy in organic solar cells, *Sci. China Chem.* 64 (4) (2021) 599–607.
- [148] X. Zhou, et al., Different morphology dependence for efficient indoor organic photovoltaics: the role of the leakage current and recombination losses, *ACS Appl. Mater. Interfaces* 13 (37) (2021) 44604–44614.
- [149] Z. Chen, et al., Trap state induced recombination effects on indoor organic photovoltaic cells, *ACS Energy Lett.* 6 (9) (2021) 3203–3211.
- [150] S. Biswas, et al., Decent efficiency improvement of organic photovoltaic cell with low acidic hole transport material by controlling doping concentration, *Appl. Surf. Sci.* 512 (2020), 145700.
- [151] B.H. Babu, et al., Modification of hole transport layers for fabricating high performance non-fullerene polymer solar cells, *Chin. J. Chem.* 38 (8) (2020) 817–822.
- [152] R. Shi, et al., Extracting energetic disorder in organic solar cells using percolation models, *ChemPhysMater* 3 (2022).
- [153] S. Biswas, et al., Efficiency improvement of indoor organic solar cell by optimization of the doping level of the hole extraction layer, *Dyes Pigments* 183 (2020), 108719.
- [154] S. Biswas, et al., Utilization of poly (4-styrenesulfonic acid) doped polyaniline as a hole transport layer of organic solar cell for indoor applications, *Thin Solid Films* 700 (2020), 137921.
- [155] Y. Lin, et al., 17% efficient organic solar cells based on liquid exfoliated WS₂ as a replacement for PEDOT:PSS, *Adv. Mater.* 31 (46) (2019), 1902965.
- [156] J. Min, et al., High-performance all-small-molecule organic solar cells without interlayers, *Energy Environ. Sci.* 14 (5) (2021) 3174–3183.
- [157] M. Ramrez-Como, et al., Small molecule organic solar cells toward improved stability and performance for Indoor Light Harvesting Application, *Sol. Energy Mater. Sol. Cells* 230 (2021), 111265.
- [158] Y. Li, Molecular Design of Photovoltaic Materials for polymer solar cells toward suitable electronic, *Acc. Chem. Res.* 45 (5) (2012) 723–733.
- [159] N. Espinosa, et al., Solar cells with one-day energy payback for the factories of the future, *Energy Environ. Sci.* 5 (1) (2012) 5117–5132.
- [160] G. Li, et al., Polymer solar cells, *Nat. Photonics* 6 (3) (2012) 153–161.
- [161] L.-K. Ma, et al., High-efficiency indoor organic photovoltaics with a band-aligned interlayer, *Joule* 4 (7) (2020) 1486–1500.
- [162] L. Tan, et al., Highly efficient flexible polymer solar cells with robust mechanical stability, *Adv. Sci.* 6 (7) (2019), 1801180.
- [163] G. Xu, Y. Li, Metal-microstructure based flexible transparent electrodes and their applications in electronic devices, *Nano Select* 1 (2) (2020) 169–182.
- [164] J. Zhang, et al., Self-doping fullerene electrolyte-based electron transport layer for all-room-temperature-processed high-performance flexible polymer solar cells, *Adv. Funct. Mater.* 28 (13) (2018), 1705847.
- [165] R. Zhu, et al., Fused silver nanowires with metal oxide nanoparticles and organic polymers for highly transparent conductors, *ACS Nano* 5 (12) (2011) 9877–9882.
- [166] T. Kim, et al., Flexible, highly efficient all-polymer solar cells, *Nat. Commun.* 6 (2015) 8547.
- [167] Z. Liang, et al., Effects of the morphology of a ZnO buffer layer on the photovoltaic performance of inverted polymer solar cells, *Adv. Funct. Mater.* 22 (10) (2012) 2194–2201.
- [168] Q.-D. Ou, et al., Enhanced light harvesting in flexible polymer solar cells: synergistic simulation of a plasmonic meta-mirror and a transparent silver mesowire electrode, *J. Mater. Chem. A* 4 (48) (2016) 18952–18962.
- [169] M.S. White, et al., Ultrathin, highly flexible and stretchable PLEDs, *Nat. Photonics* 7 (10) (2013) 811–816.
- [170] S. Ye, et al., Metal nanowire networks: the next generation of transparent conductors, *Adv. Mater.* 26 (39) (2014) 6670–6687.
- [171] X. Liu, et al., Fluidic manipulating of printable zinc oxide for flexible organic solar cells, *Adv. Mater.* 34 (3) (2022), 2106453.
- [172] Z. Peng, et al., Thermoplastic elastomer tunes phase structure and promotes stretchability of high-efficiency organic solar cells, *Adv. Mater.* (2021), 2106732.
- [173] F. Yang, et al., Large-area flexible organic solar cells, *npj Flex. Electron.* 5 (1) (2021) 30.
- [174] T. Yokota, et al., Ultraflexible organic photonic skin, *Sci. Adv.* 2 (4) (2016), 1501856.
- [175] A. Ghanbari, et al., A novel approach to control thermal degradation of PET/organoclay nanocomposites and improve clay exfoliation, *Polymer* 54 (4) (2013) 1361–1369.
- [176] W. Song, et al., Foldable semitransparent organic solar cells for photovoltaic and photosynthesis, *Adv. Energy Mater.* 10 (15) (2020), 2000136.
- [177] H. Yin, et al., Thick-film low driving-force indoor light harvesters, *Sol. RRL* 4 (10) (2020), 2000291.
- [178] W. Pan, et al., Over 1 cm² flexible organic solar cells, *J. Semiconduct.* 42 (5) (2021), 050301.
- [179] R. Sun, et al., PEDOT:PSS-Free polymer non-fullerene polymer solar cells with efficiency up to 18.60% employing a binary-solvent-chlorinated ITO anode, *Adv. Funct. Mater.* 31 (51) (2021), 2106846.
- [180] X. Chen, et al., Realizing ultrahigh mechanical flexibility and >15% efficiency of flexible organic solar cells via a "welding" flexible transparent electrode, *Adv. Mater.* 32 (14) (2020), 1908478.
- [181] Z. Chen, et al., Small-molecular donor guest achieves rigid 18.5% and flexible 15.9% efficiency organic photovoltaic via fine-tuning microstructure morphology, *Joule* 5 (9) (2021) 2395–2407.
- [182] J. Huang, et al., Seed-layer-free growth of ultra-thin Ag transparent conductive films imparts flexibility to polymer solar cells, *Sol. Energy Mater. Sol. Cells* 184 (2018) 73–81.
- [183] Q. Kang, et al., A printable organic cathode interlayer enables over 13% efficiency for 1-cm² organic solar cells, *Joule* 3 (1) (2019) 227–239.
- [184] D. Koo, et al., Flexible organic solar cells over 15% efficiency with polyimide-integrated graphene electrodes, *Joule* 4 (5) (2020) 1021–1034.
- [185] K. Li, et al., Versatile biomimetic haze films for efficiency enhancement of photovoltaic devices, *J. Mater. Chem. B* 5 (3) (2017) 969–974.

- [186] X. Lu, et al., Metal-based flexible transparent electrodes: challenges and recent advances, *Adv. Electron. Mater.* 7 (5) (2021), 2001121.
- [187] X. Meng, et al., A general approach for lab-to-manufacturing translation on flexible organic solar cells, *Adv. Mater.* 31 (41) (2019), 1903649.
- [188] F. Qin, et al., 54 cm² large-area flexible organic solar modules with efficiency above 13, *Adv. Mater.* 33 (39) (2021), 2103017.
- [189] J. Wan, et al., Metal oxide-free flexible organic solar cells with 0.1 M perchloric acid sprayed polymeric anodes, *J. Mater. Chem. S* 8 (40) (2020) 21007–21015.
- [190] J. Wan, et al., All annealing-free solution-processed highly flexible organic solar cells, *J. Mater. Chem. S* 9 (9) (2021) 5425–5433.
- [191] Y. Li, et al., Flexible and semitransparent organic solar cells, *Adv. Energy Mater.* 8 (7) (2018), 1701791.
- [192] X. Zheng, et al., High-efficiency ITO-free organic photovoltaics with superior flexibility and upscalability, *Adv. Mater.* (2022), 2200044.
- [193] X. Duan, et al., Ternary strategy enabling high-efficiency rigid and flexible organic solar cells with reduced non-radiative voltage loss, *Energy Environ. Sci.* 15 (4) (2022) 1563–1572.
- [194] H. Ghasemi, et al., Properties of PET/clay nanocomposite films, *Polym. Eng. Sci.* 52 (2) (2012) 420–430.
- [195] J. Huang, et al., Stretchable ITO-free organic solar cells with intrinsic anti-reflection substrate for high-efficiency outdoor and indoor energy harvesting, *Adv. Funct. Mater.* 31 (16) (2021), 2010172.
- [196] W. Zheng, et al., Efficient low-cost all-flexible microcavity semitransparent polymer solar cells enabled by polymer flexible one-dimensional photonic crystals, *ACS Appl. Mater. Interfaces* 12 (20) (2020) 23190–23198.
- [197] Z. Hu, et al., A critical review on semitransparent organic solar cells, *Nano Energy* 78 (2020), 105376.
- [198] P. Cheng, et al., Transparent hole-transporting frameworks: a unique strategy to design high-performance semitransparent organic photovoltaics, *Adv. Mater.* 32 (39) (2020), 2003891.
- [199] J. Wan, et al., Solution-processed transparent conducting electrodes for flexible organic solar cells with 16.61% efficiency, *Nano-Micro Lett.* 13 (1) (2021) 44.
- [200] Y. Chang, et al., Regioregular narrow bandgap copolymer with strong aggregation ability for high-performance semitransparent photovoltaics, *Nano Energy* 86 (2021), 106098.
- [201] Y. Xie, et al., Fibril network strategy enables high-performance semitransparent organic solar cells, *Adv. Funct. Mater.* 30 (28) (2020), 2002181.
- [202] C. Xu, et al., Efficient semitransparent layer-by-layer organic photovoltaics via optimizing wide bandgap and narrow absorption polymer layer thickness, *Sol. RRL* (2022), 2200308.
- [203] G. Xu, et al., High-performance colorful semitransparent polymer solar cells with ultrathin hybrid-metal electrodes and fine-tuned dielectric mirrors, *Adv. Funct. Mater.* 27 (15) (2017), 1605908.
- [204] J. Zhang, et al., Highly efficient semitransparent organic solar cells with color rendering index approaching 100, *Adv. Mater.* 31 (10) (2019), 1807159.
- [205] Z. Hu, et al., Semitransparent polymer solar cells with 9.06% efficiency and 27.1% average visible transmittance obtained by employing a smart strategy, *J. Mater. Chem. S* 7 (12) (2019) 7025–7032.
- [206] X. Ma, et al., Simultaneously improved efficiency and average visible transmittance of semitransparent polymer solar cells with two ultra-narrow bandgap nonfullerene acceptors, *J. Mater. Chem. S* 6 (43) (2018) 21485–21492.
- [207] Z. Hu, et al., Semitransparent ternary nonfullerene polymer solar cells exhibiting 9.40% efficiency and 24.6% average visible transmittance, *Nano Energy* 55 (2019) 424–432.
- [208] C. Xu, et al., Wide bandgap polymer with narrow photon harvesting in visible light range enables efficient semitransparent organic photovoltaics, *Adv. Funct. Mater.* 31 (52) (2021), 2107934.
- [209] Z. Hu, et al., Semitransparent polymer solar cells with 12.37% efficiency and 18.6% average visible transmittance, *Sci. Bull.* 65 (2) (2020) 131–137.
- [210] R.F. Bailey-Salzman, et al., Semitransparent organic photovoltaic cells, *Appl. Phys. Lett.* 88 (23) (2006), 233502.
- [211] C. Chueh, et al., Toward high-performance semi-transparent polymer solar cells: optimization of ultra-thin light absorbing layer and transparent cathode architecture, *Adv. Energy Mater.* 3 (4) (2013) 417–423.
- [212] J. Huang, et al., A semi-transparent plastic solar cell fabricated by a lamination process, *Adv. Mater.* 20 (3) (2008) 415–419.
- [213] S.K. Hau, et al., Indium tin oxide-free semi-transparent inverted polymer solar cells using conducting polymer as both bottom and top electrodes, *Org. Electron.* 10 (7) (2009) 1401–1407.
- [214] A.K. Pandey, I.D.W. Samuel, Photophysics of solution-processed transparent solar cells under top and bottom illumination, *IEEE J. Sel. Top. Quant. Electron.* 16 (6) (2010) 1560–1564.
- [215] M.B. Upama, et al., High performance semitransparent organic solar cells with 5% PCE using non-patterned MoO₃/Ag/MoO₃ anode, *Curr. Appl. Phys.* 17 (2) (2017) 298–305.
- [216] W. Yu, et al., Highly efficient and high transmittance semitransparent polymer solar cells with one-dimensional photonic crystals as distributed Bragg reflectors, *Org. Electron.* 15 (2) (2014) 470–477.
- [217] B.R. Photosensitizers, Of the porphyrin and phthalocyanine series for photodynamic therapy, *ChemInform* 26 (37) (1995) 19–33.
- [218] J.G. Straka, et al., Porphyrin and porphyrin metabolism, *Annu. Rev. Med.* 41 (1) (1990) 457–469.
- [219] Aswani Yella, et al., Porphyrin sensitized solar cells with cobalt based redox electrolyte exceed 12 percent efficiency, *Science* 334 (6056) (2011) 629–634.
- [220] L.L. Li, E.W. Diau, Porphyrin-sensitized solar cells, *Chem. Soc. Rev.* 42 (1) (2013) 291–304.
- [221] S. Chen, et al., Solution-processed new porphyrin-based small molecules as electron donors for highly efficient organic photovoltaics, *Chem. Commun.* 51 (77) (2015) 14439–14442.
- [222] K. Gao, et al., Deep absorbing porphyrin small molecule for high-performance organic solar cells with very low energy losses, *J. Am. Chem. Soc.* 137 (23) (2015) 7282–7285.
- [223] B. Zhao, et al., Flexible polymer solar cells with power conversion efficiency of 8.7%, *J. Mater. Chem. C* 2 (26) (2014) 5077–5082.
- [224] H. Yin, et al., Highly-transparent and true-colored semitransparent indoor photovoltaic cells, *Small Methods* 4 (8) (2020), 2000136.